Minimal "Self" Peptides That Inhibit Phagocytic Clearance and Enhance Delivery of Nanoparticles

Pia L. Rodriguez,[1] Takamasa Harada,[1] David A. Christian,[1] Diego A. Pantano,[1] Richard K. Tsai,[1] Dennis E. Discher[1,2]*

Foreign particles and cells are cleared from the body by phagocytes that must also recognize and avoid clearance of "self" cells. The membrane protein CD47 is reportedly a "marker of self" in mice that impedes phagocytosis of self by signaling through the phagocyte receptor CD172a. Minimal "Self" peptides were computationally designed from human CD47 and then synthesized and attached to virus-size particles for intravenous injection into mice that express a CD172a variant compatible with hCD47. Self peptides delay macrophage-mediated clearance of nanoparticles, which promotes persistent circulation that enhances dye and drug delivery to tumors. Self-peptide affinity for CD172a is near the optimum measured for human CD172a variants, and Self peptide also potently inhibits nanoparticle uptake mediated by the contractile cytoskeleton. The reductionist approach reveals the importance of human Self peptides and their utility in enhancing drug delivery and imaging.

Macrophages evolved to engulf and clear invading microbes and dying cells, but they respond similarly to injected particles, viruses, and implants, which hampers delivery of therapeutics and imaging agents. Coating of nanoparticles or liposomes with polyethylene glycol (PEG) creates "stealth" brushes that mimic a cell's glycocalyx and that delay immune clearance of foreign particles (*1*–*3*), but brushes can also hinder uptake by diseased cells (*4*). Neither a polymer brush nor a glycocalyx stops adsorption of abundant serum proteins, such as immunoglobulin G (IgG) (table S1), which promote clearance [e.g., (*1*–*3*, *5*)], and any foreign polymer can also be immunogenic (*6*). Targeting diseased cells with ligand-modified particle constructs might make brushes unnecessary, but some ligands also promote rapid clearance by phagocytes (*2*, *7*). In the reductionist approach here, we make a synthetic, human-based "Self" peptide that specifically binds and signals to phagocytes to inhibit clearance of particles as small as viruses.

CD47 glycoprotein is a putative "marker of self" in mice (*8*) and is expressed on all cell membranes in humans, mice, and other mammals (*9*). It associates in cis with integrins (*10*) and other species-specific, immunogenic complexes on cells (*11*–*13*). Mouse knockouts of CD47 (mCD47) are viable, but when red blood cells (mRBCs) from these mice are injected into the circulation of control mice, the deficient cells are cleared within hours by splenic macrophages, whereas normal mRBCs circulate for weeks (*8*). CD47's extracellular domain interacts with CD172a (also known as signal regulatory protein-α, SIRPα) on phagocytes (*10*). Although binding is typically species-restricted (*13*), SIRPα is highly polymorphic, even within a species (*14*). Macrophages in nonobese diabetic/severe combined immunodeficient (NOD/SCID) strains of mice express a SIRPα variant that cross-reacts with human CD47 (hCD47), which explains why human hematopoietic cells engraft and circulate in NOD/SCID better than any other mice (*14*, *15*). In vitro, the CD47-SIRPα interaction inhibits mouse macrophage uptake of antibody-coated mRBCs (*8*), as well as human macrophage uptake of both human RBCs (hRBCs) and hCD47-coated microparticles (*16*). This is not surprising as SIRPα signaling inhibits contractility-driven uptake of micron-size cells and particles (*16*). However, contractile forces are widely considered unimportant to internalization of nanoparticles and viruses, and so it is unclear whether this inhibitory interaction could be exploited in nanoparticle-based therapeutics.

We addressed whether hCD47 and a synthetic Self peptide can minimize phagocytic uptake of nanoparticles and thereby enhance delivery in NOD/SCID mice with X-linked severe combined immunodeficiency (*Il2rg*$^{-/-}$) mice (NSG). We first showed that blocking mCD47 accelerates clearance of mRBCs in NSG mice. Cells (or nanobeads) were split into two samples, with one sample labeled by red fluorophore and the other sample labeled by far-red fluorophore plus antibody against mCD47. The samples were mixed 1:1 for injection into the same mouse, and blood samples at subsequent time points were analyzed by flow cytometry for both colors, which produced a ratio (fig. S1A) that minimizes mouse-to-mouse variations. IgG and other serum proteins physisorb in vivo to RBCs (*17*), viruses (*18*), and PEGylated nanoparticles (*19*) (table S1), but in NSG mice, IgG is very low or not detectable (versus ~100 μM in normal animals). Controlled opsonization with IgG was therefore used in most of our studies to better mimic immune-competent animals. With RBCs, mRBC-specific antibody was added to promote clearance via phagocytosis (*20*). Consistent with a marker-of-self function of mCD47, the persistence ratio for the mixed sample [mRBCs/(mRBCs with blocked mCD47)] increased exponentially with a doubling time (T) of 33 min (Fig. 1B); single-color analyses also give T = 30 min (fig. S1B).

[1]Molecular and Cell Biophysics and NanoBioPolymers Laboratory, University of Pennsylvania, Philadelphia, PA 19104, USA. [2]Pharmacological Sciences Graduate Group, University of Pennsylvania, Philadelphia, PA 19104, USA.

*To whom correspondence should be addressed. E-mail: discher@seas.upenn.edu

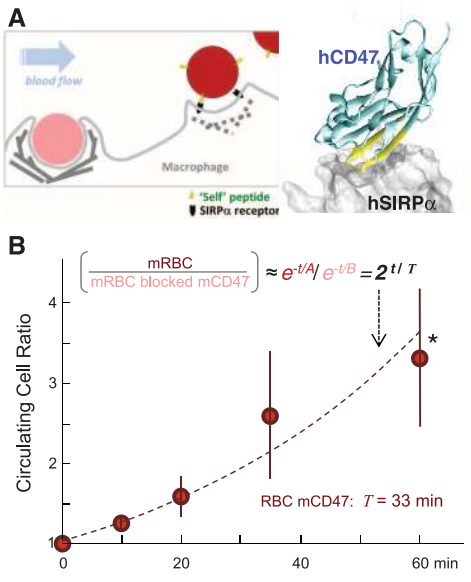

Fig. 1. Self peptide and hCD47 prolong the circulation of nanobeads in NSG mice. (**A**) Competitive circulation in which two colors of nanobeads or cells injected into the same mouse are flowing with blood and being cleared by a splenic macrophage (left) or else recognized as self and released (right). Blood was sampled periodically in the experiment (50 μl), and flow cytometry analysis yields the bead or cell ratio in each mouse at each time point. The cocrystal structure shows hCD47 with the Self peptide binding hSIRPα. (**B**) Competitive circulation experiment in which mRBCs from NSG mice were either blocked with anti-CD47 or not and were also opsonized with excess mRBC-specific antibody before cells were mixed together and injected into the tail vein. Both color cell types are cleared with clearance constants ~*A* or *B* (*A* > *B*), and the ratio of exponentials gives the persistence ratio doubling time *T* (n = 3 mice; R^2 = 0.93 for fit of means with indicated *T*). (**C**) Circulation experiments used 160-nm polystyrene beads with covalently attached streptavidin incubated with biotinylated versions of one of the following: synthetic Self peptide (n = 4; R^2 = 0.94 for fit of means); recombinant hCD47 (n = 6; R^2 = 0.92 for fit of means); or negative controls of either Scrambled peptide (n = 3) or PEG (n = 5). Nanobeads were also opsonized with streptavidin-specific antibody, and then 10^7 were injected. Flow cytometry quantification was typically done on 100 to 10,000 particles at each time point and typically included quantification of both hCD47 and opsonin on the nanobeads. For hCD47 and Self peptide, a separate fit for each mouse gives the indicated mean *T* ± SEM for each group, which is within 10% of the *T* obtained from fitting the group averages (dashed curves). Most data points for hCD47 and Self peptide differ significantly from PEG-nanobeads (*P < 0.05). All data are means ± SEM.

RBC membranes have hundreds of different interacting proteins, and many involved in clearance are different for mouse and humans (*12*, *21*). To give a better-defined surface for reductionist studies in vivo and also to begin testing the marker-of-Self concept on foreign particles of potential use for imaging and therapy, the extracellular immunoglobulin-like domain of hCD47, which binds SIRPα, was recombinantly expressed; site-specifically biotinylated; and then bound to streptavidin-coated, 160-nm polystyrene nanobeads. Beads were also labeled with red or near-infrared dyes (or left unlabeled) and controllably opsonized with either antibody against streptavidin (fig. S1C) or a biotinylated antibody for targeting (fig. S1D). After injection into an NSG mouse, blood analysis by flow cytometry clearly identified nanobeads on the basis of both distinctive scatter and fluorescence detection of the opsonizing antibody ± hCD47 (Fig. 1A and fig. S1, A and C). A persistence ratio for [(nanobead + hCD47)/nanobead] was well-controlled at every time point and again increased exponentially with a doubling time (*T*) of 33 ± 8 min (Fig. 1C). Mice injected with a single color of nanobead gave similar results (*T* = 31 min) (fig. S1E). PEG-biotin nanobeads that were also preopsonized showed a flat persistence curve (*T* > 200 min), consistent with the fact that PEG brushes alone do not directly inhibit clearance by macrophages (fig. S2, A to C). In the absence of preopsonization, PEG-nanobeads did circulate for hours as expected, but hCD47, once again, enhanced circulation (fig. S2D). hCD47 on virus-size particles is thus an inhibitor of in vivo clearance and thereby prolongs circulation.

Minimization of the 117–amino acid immunoglobulin-like domain of hCD47 to a small, binding-site Self peptide could provide key evidence that signaling to mouse SIRPα (mSIRPα) is part of the molecular mechanism for inhibiting clearance in vivo. A crystal structure of hCD47-hSIRPα suggests three distinct binding sites (*22*), but the highest density of interactions are in one loop in hCD47 between canonical β strands F and G, where a nine–amino acid sequence constitutes 40% of hCD47's contacting residues (Fig. 1A, structure). We designed by simulation a 21–amino acid Self peptide around this sequence with the aims of minimizing species specificity (*13*) and eliminating glycosylation of CD47, which impedes binding (*23*). Biotinylation on an amino-terminal PEG linker provided a means of attachment to streptavidin beads for in vivo studies. Relative to control nanobeads, the Self peptide increased the persistence of beads in the circulation with a mean doubling time, *T*, of 20 ± 3 min, whereas Scrambled peptide (see supplementary materials) had little impact on circulation (Fig. 1C). An apparent difference in persistence in the circulation between Self peptide and hCD47 is not significant (P = 0.18).

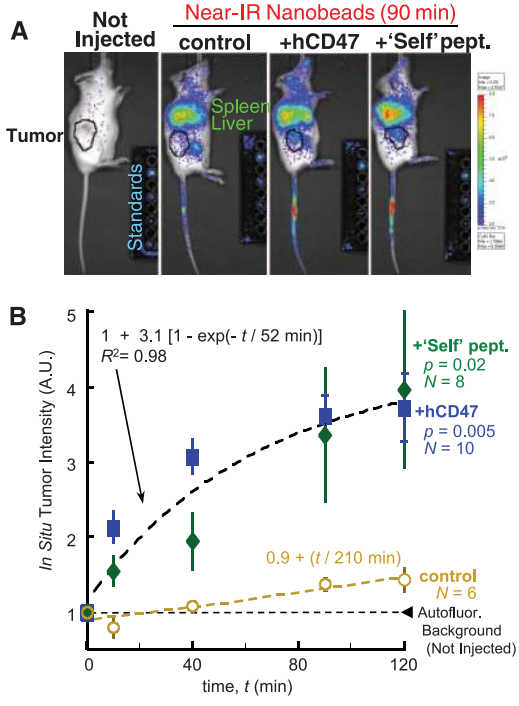

Fig. 2. Self peptide and hCD47 enhance tumor imaging by near-infrared particles. (**A**) NSG mice with flank tumors of A549 lung–derived cells (black circles) received tail vein injections of nanobead mixtures in which one bead type is labeled with DiR fluorophore. Images of live mice and calibration standards were taken with a Xenogen imager. Tumor-bearing mice have persistence ratios of particles in blood at 35 min, similar to results in Fig. 1C, even though many particles are seen in spleen and liver. (**B**) The tumor was located by bright-field imaging, and total fluorescence was quantified at each time point. All results for Self peptide and hCD47 were combined in the fit. *N*, Number of tumors from three different sets of tumor-bearing mice. All data are means ± SEM.

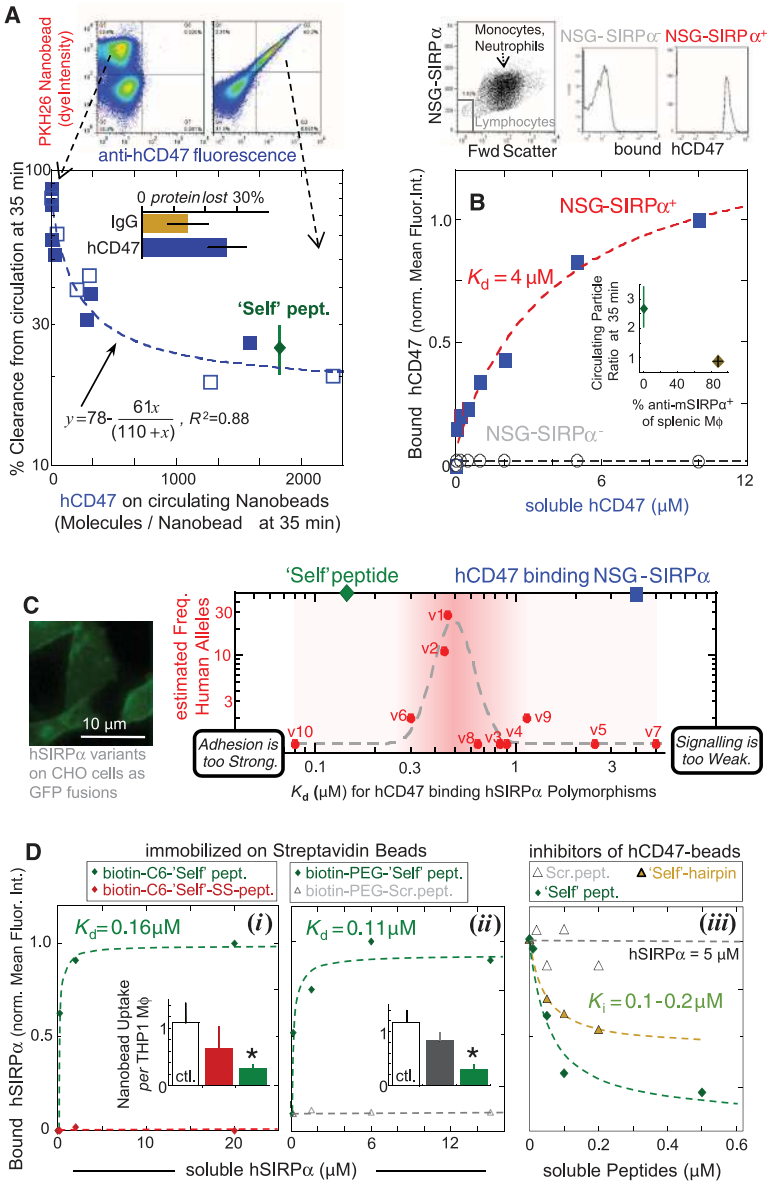

Fig. 3. Persistence of hCD47 and Self nanobeads depends on hCD47 density, consistent with low-affinity binding to NSG mSIRPα relative to hSIRPα variants. (**A**) The number of hCD47 molecules on the 160-nm beads 35 min after injection was either measured in two-color experiments (solid symbols; n = 7 mice) or single-color experiments (open symbols; n = 6 mice), with an average of 30% protein lost in circulation (inset). Self peptide levels are estimated to have a similar loss (n = 4 mice). Fluorescent nanobeads (PKH26$^+$ in flow cytometry, top) were confirmed by forward and/or side scatter, and fluorescent hCD47-specific antibody measured hCD47 levels (left, control nanobead sample; right, hCD47 nanobead sample). The inhibition curve gives K_i = 110 molecules/nanobead. (**B**) Affinity of soluble hCD47 for NSG neutrophils and monocytes, from flow cytometry analysis of Cy5-biotin–specific antibody. Lymphocytes are negative for SIRPα and do not bind soluble hCD47. (Inset) Preinjection of blocking anti-mSIRPα eliminates the enhanced circulation of Self nanobeads of Fig. 1C. After 35 min, most splenic macrophages (Mϕ: F4/80 antibody+) have mSIRPα antibody on their surface (n = 4 mice). (**C**) Ten reported variants of hSIRPα's N-terminal domain (*14*) were displayed on CHO cells to determine effective K_d values for soluble hCD47; soluble hSIRPα binding to hCD47 beads showed the same trend (fig. S7E). The putative allele frequency (*14*) is highest at intermediate K_d, whereas the affinity of hCD47 for mSIRPα on NSG phagocytes (blue square) is weaker and that of Self peptide for hSIRPα(v1) is stronger (green diamond). The Lorentzian fit is inspired by other mechanobiological signaling processes and has the form: $y = 1 + 0.05x^{11}/(0.50^{11} + x^{11})^2$, R^2 = 0.85. (**D**) Binding of peptides on beads to soluble hSIRPα (v1) was assayed by flow cytometry. Neither the Self-SS peptide with a T107C substitution nor the Scrambled peptide bind hSIRPα. The assays in (*iii*) use soluble peptides and show the 10–amino acid Self hairpin centered on the loop is a partial inhibitor. Bar graph insets in (*i* and *ii*) show in vitro phagocytosis assay results with the human THP1 cell line, which demonstrates that only the Self peptide (attached to biotin via either PEG or C6, 6-aminohexanoic acid) significantly inhibits phagocytic uptake (*P < 0.05 different from control). All data are means ± SEM.

Prolonged circulation of hCD47 beads and Self beads is based on a delay of phagocytic clearance by the spleen and perhaps liver, but nanobeads localize nonetheless to these organs in whole-body imaging of near-infrared fluorescent (NIRF) beads (Fig. 2A and fig. S3, A to D) by interactions that are likely similar to those that promote RBC adhesion in spleen and greatly increase splenic hematocrit (*24*). Recombinant mCD47 also enhanced persistence in circulation and again showed moderate but suppressed splenic localization (fig. S3B). For additional insight into persistent circulation and potential therapeutic application of Self-nanoparticles, human-derived A549 lung adenocarcinoma epithelial cells were grafted into the flanks of NSG mice, NIRF nanobeads were injected into the tail veins weeks later, and the tumors were imaged both in vivo and ex vivo to quantify accumulated signal. As early as 10 min post injection, hCD47 and Self nanobeads gave mean tumor intensities twice those of noninjected mice, whereas control beads gave background-level signal (Fig. 2B). With hCD47 and Self nanobeads, the fluorescence at every time point is statistically similar but significantly higher than that of control beads (P < 0.05), and the increase fits first-order kinetics (τ = 52 min), consistent with enhanced perfusion and progressive clearance. At 40 min, both hCD47 and Self nanobeads give higher signals than controls, ~10 to 20 times as much, and a second injection of hCD47 nanobeads after 2 hours showed a similar signal increase (fig. S4, A and B). Tumor accumulation fits a first-order process (with τ = 52 min giving $T = \tau \ln 2$ = 36 min) that is much faster than control beads (T = 210 min), and both time scales are similar to those obtained for persistent circulation (Fig. 1C), consistent with the hypothesis that enhanced tumor signal results from persistent circulation.

After in situ imaging, tumors and other major organs were subsequently excised and imaged ex vivo (fig. S4C). The Self beads and hCD47 beads show at least 16- to 22-fold enhancement of the very low signals obtained with control beads either with or without Scrambled peptide, with no statistical difference between Self peptide and hCD47. The fraction of nanobeads in the blood within the tumor is small (fig. S4C, inset), and so the majority of signal derives from beads that have accumulated in the tumor, most likely by enhanced permeation and retention (EPR) through the leaky vasculature that is characteristic of many solid tumors (*25*). On the basis of these results, the hydrophobic anticancer drug paclitaxel (Tax) was loaded into the Self nanobeads, as well as into beads with PEG and/or antibody against hCD47 (fig. S5, A and B). The latter antibodies have been used therapeutically to mask self on cancer cells (*26*), but targeting antibodies are a double-edged sword when attached to beads, because they also promote clearance (fig. S1D). Tax-loaded beads that displayed either recombinant hCD47 (fig. S5C) or Self-peptide plus PEG and hCD47-targeting antibody (fig. S5D) consistently shrank tumors more than beads lacking Self. The Self beads also did as well or better than the standard paclitaxel

nanocarrier Cremophore, which is known for its toxic side effects (e.g., fig. S5, E and F). The NSG mouse results thus reveal active suppression of clearance by both hCD47 and Self peptide, which could enhance both tumor imaging and drug delivery.

Flow cytometry enables detailed analysis of the surface of nanobeads sampled from circulation. Although streptavidin-specific IgG remains stably bound, biotinylated hCD47 is partially lost (30% in Fig. 3A, inset bar graph; fig. S6A). Nonetheless, the percentage clearance of nanobeads at 35 min versus the measured density of hCD47 at 35 min fits an inhibition model (Fig. 3A) with the inhibition constant $K_{i,in\text{-}vivo}$ of 110 molecules per 160-nm nanobead. This appears independent of circulating bead number over at least a ~10-fold range (fig. S6B). This $K_{i,in\text{-}vivo}$ corresponds to a density of hCD47 that is 10 times that of the lowest densities reported for hRBCs [~25 hCD47 molecules/μm^2 (*12*)] but ~1/100th of nanobead saturation (e.g., fig. S2A). Although binding of soluble hCD47 to NSG-SIRPα$^+$ phagocytes yields a weak affinity (K_d = 4 μM) (Fig. 3B), lymphocytes, which do not express SIRPα (*27*), show zero binding. In vivo evidence of interaction specificity was also obtained by preinjecting mSIRPα-specific antibody, which blocks hCD47 binding, followed by injection of Self nanobeads; these beads were cleared as if lacking Self (Fig. 3B, inset).

To compare the effective affinity of NSG mouse to human SIRPα (hSIRPα), 10 human polymorphic variants of hSIRPα (*14*) were expressed on Chinese hamster ovary (CHO) cell membranes (*24*). Saturation binding of soluble hCD47 to each variant yielded a 60-fold range of affinities with K_d = 0.08 to 5 μM (Fig. 3C and fig. S7), even though all of the amino acid differences in the variants are outside of the binding interface (*22*). When plotted against the allele frequency of hSIRPα, variants of intermediate affinity (e.g., v1 and v2) are most common, with affinities similar to that for soluble SIRPα(v1) binding to CHO-displayed hCD47 (*23*). hCD47's affinity for NSG-SIRPα phagocytes is within the range of reported hSIRPα variants and so is the affinity of Self peptide for the most common SIRPα variant. Synthesis and simulations of additional peptides (Fig. 3D and fig. S8) reveal a sensitivity of binding to conformation, as well as sequence, and show that a lack of affinity for hSIRPα is predictive of a failure to inhibit in vitro phagocytosis.

Whether phagocytosis of nanoparticles—including viruses—involves mechanisms similar to those for larger particles remains an open question (*28*). Tissue sections show that nanobeads colocalize with macrophages (Fig. 4A, *i*). In cultures of human-derived monocytic cell line THP1 macrophages, nanoparticles are not dense enough to settle and contact cells, but opsonized nanobeads that are added at the same total surface area as microbeads (fig. S9A) are taken up with equal efficiency (Fig. 4A, *ii*, *a*). Myosin-II accumulates at the phagocytic synapse formed with opsonized beads except when hCD47 is attached (Fig. 4A, *ii*, *a* and *b*). Microparticles and microbes (i.e., bacteria) give similar images (fig. S9B), and inhibition of phagocytic uptake by hCD47 is indeed independent of particle size from at least 100 nm to 10 μm (Fig. 4A, *ii*, *c*; and fig. S9C). Similar inhibition of nanobead uptake was found with biotinylated Self peptides, whereas both Scrambled peptide and disulfide-bridged peptide (Self-SS) showed no significant inhibition of uptake (Fig. 3D, *i* and *ii*). The potency of hCD47 is remarkable with $K_{i,in\text{-}vitro} \approx 1.0 \pm 0.3$ molecule per 45,000 nm^2. Equivalently, a nanoparticle of 60-nm radius requires only one CD47 molecule to inhibit uptake. $K_{i,in\text{-}vitro}$ is the same as the lowest densities reported for hRBCs (*12*) and is far smaller than PEG densities needed to enhance nanoparticle circulation through delayed opsonization (e.g., fig. S2A: >1 PEG per 20 nm^2).

IgG-driven uptake is linear in myosin-II activity (*16*). With the nanobeads described here, both drug inhibition of myosin-II and hCD47 inhibit uptake by up to 80% (Fig. 4A, *ii*, *c*). When CD47 binds SIRPα, SIRPα's cytoplasmic tail is hyperphosphorylated to activate SHP1 phosphatase (*29*), which dephosphorylates multiple proteins, including myosin-II (*16*). Inhibition of SHP1 produces the expected increase in phagocytosis of hCD47 beads (Fig. 4A, *ii*, *c*; and fig. S9D), and binding of hCD47 and Self peptide indeed increases phospho-SIRPα (Fig. 4B). Consistent with a common mechanism in vitro and in vivo, uptake of the various nanoparticles by THP1 cells correlates inversely with persistence in NSG mice (Fig. 4C).

Phagocytes pervade all tissues and disease sites, with key roles in recognition and clearance, as well as contributions to pro- and anti-inflammatory responses with cytokine release and oxidative burst. Whether synthetic Self peptides, CD47, or its homologs are displayed on particles, viruses (*30*), or artificial surfaces (*31*), "active stealth" signaling across length scales (fig. S10) offers additional opportunities in application as well as understanding. In particular, the SIRPα polymorphism results suggest that an intermediate affinity for Self is optimal (Fig. 3C) as a trade-off between adhesion that is not too strong ("must let go") and signaling that is not too weak ("don't eat me"). Additional homeostatic self factors seem likely and might similarly be used to further avoid phagocytes and thereby enhance delivery of therapeutics and imaging agents.

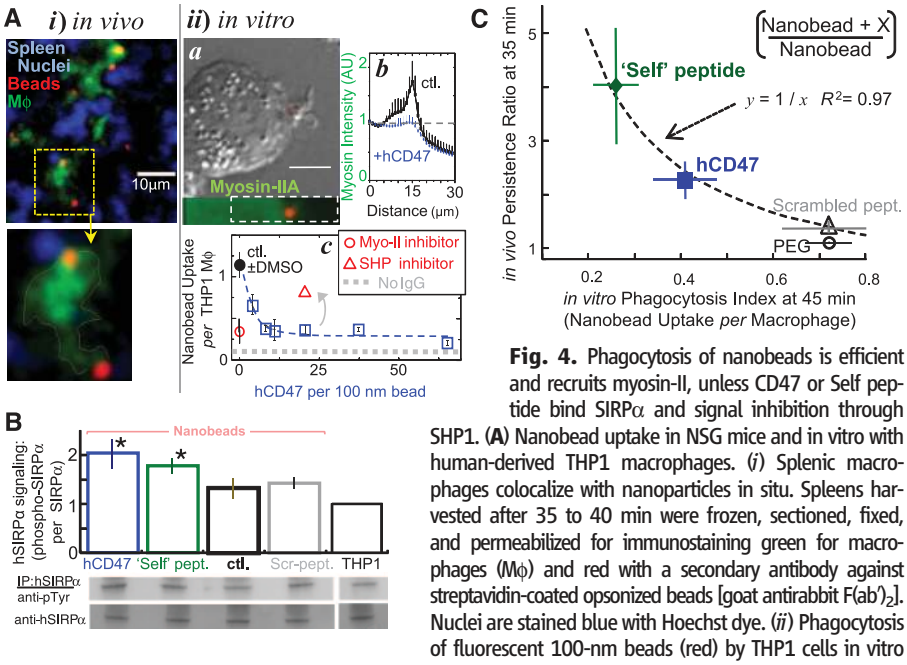

Fig. 4. Phagocytosis of nanobeads is efficient and recruits myosin-II, unless CD47 or Self peptide bind SIRPα and signal inhibition through SHP1. (**A**) Nanobead uptake in NSG mice and in vitro with human-derived THP1 macrophages. (*i*) Splenic macrophages colocalize with nanoparticles in situ. Spleens harvested after 35 to 40 min were frozen, sectioned, fixed, and permeabilized for immunostaining green for macrophages (Mϕ) and red with a secondary antibody against streptavidin-coated opsonized beads [goat antirabbit F(ab')$_2$]. Nuclei are stained blue with Hoechst dye. (*ii*) Phagocytosis of fluorescent 100-nm beads (red) by THP1 cells in vitro was assessed at 45 min by immunostaining cultures that were fixed (but not cell permeabilized) for noningested beads by using secondary antibody against antistreptavidin. Nonmuscle myosin-IIA (*a*, bottom) enriches near the nanoparticle unless hCD47 is on the bead (*b*, plot). Enrichment extends deeply into the cytoplasm (~5 μm) relative to bead size, suggestive of a diffuse signal that directs cytoskeletal assembly. Nanobeads with antistreptavidin are readily engulfed at about 1 bead per cell (*c*), but uptake is inhibited by hCD47 and by inhibition of myosin-IIA with blebbistatin (50 μM). Inhibition of SHP1, downstream of SIRPα, with NSC-87877 blocks the inhibition of uptake by hCD47. Dimethyl sulfoxide (DMSO) is the solvent for the drugs. (**B**) Phosphorylation of hSIRPα tyrosines in THP1 cells upon contact with opsonized nanobeads bearing hCD47 and Self peptide. hSIRPα was immunoprecipitated from cell lysates, and phosphotyrosine was immunoblotted for quantification (n = 3; *P < 0.05). (**C**) Inverse correlation between in vivo persistence ratio at 35 min and in vitro inhibition of phagocytosis by hCD47 and Self peptide at 45 min for 160-nm beads. All data are means ± SEM.

References and Notes

1. D. W. Bartlett, H. Su, I. J. Hildebrandt, W. A. Weber, M. E. Davis, *Proc. Natl. Acad. Sci. U.S.A.* **104**, 15549 (2007).
2. A. L. Klibanov, K. Maruyama, A. M. Beckerleg, V. P. Torchilin, L. Huang, *Biochim. Biophys. Acta* **1062**, 142 (1991).
3. P. J. Photos, L. Bacakova, B. Discher, F. S. Bates, D. E. Discher, *J. Control. Release* **90**, 323 (2003).
4. R. L. Hong *et al.*, *Clin. Cancer Res.* **5**, 3645 (1999).

5. R. Rossin, S. Muro, M. J. Welch, V. R. Muzykantov, D. P. Schuster, *J. Nucl. Med.* **49**, 103 (2008).
6. J. K. Armstrong *et al*., *Cancer* **110**, 103 (2007).
7. M. J. Turk, D. J. Waters, P. S. Low, *Cancer Lett.* **213**, 165 (2004).
8. P. A. Oldenborg *et al*., *Science* **288**, 2051 (2000).
9. A. A. Bentley, J. C. Adams, *Mol. Biol. Evol.* **27**, 2187 (2010).
10. E. J. Brown, W. A. Frazier, *Trends Cell Biol.* **11**, 130 (2001).
11. L. J. Bruce *et al*., *Blood* **101**, 4180 (2003).
12. I. Mouro-Chanteloup *et al*., *Blood* **101**, 338 (2003).
13. S. Subramanian, R. Parthasarathy, S. Sen, E. T. Boder, D. E. Discher, *Blood* **107**, 2548 (2006).
14. K. Takenaka *et al*., *Nat. Immunol.* **8**, 1313 (2007).
15. T. Strowig *et al*., *Proc. Natl. Acad. Sci. U.S.A.* **108**, 13218 (2011).
16. R. K. Tsai, D. E. Discher, *J. Cell Biol.* **180**, 989 (2008).
17. F. Turrini, F. Mannu, P. Arese, J. Yuan, P. S. Low, *Blood* **81**, 3146 (1993).
18. D. Wilflingseder *et al*., *J. Immunol.* **178**, 7840 (2007).
19. M. Lundqvist *et al*., *Proc. Natl. Acad. Sci. U.S.A.* **105**, 14265 (2008).
20. D. Cox, S. Greenberg, *Semin. Immunol.* **13**, 339 (2001).
21. A. M. Glodek *et al*., *Blood* **116**, 6063 (2010).
22. D. Hatherley *et al*., *Mol. Cell* **31**, 266 (2008).
23. S. Subramanian, E. T. Boder, D. E. Discher, *J. Biol. Chem.* **282**, 1805 (2007).
24. I. C. MacDonald, E. E. Schmidt, A. C. Groom, *Microvasc. Res.* **42**, 60 (1991).
25. Y. Matsumura, H. Maeda, *Cancer Res.* **46**, 6387 (1986).
26. S. B. Willingham *et al*., *Proc. Natl. Acad. Sci. U.S.A.* **109**, 6662 (2012).
27. M. Seiffert *et al*., *Blood* **94**, 3633 (1999).
28. J. A. Swanson, A. D. Hoppe, *J. Leukoc. Biol.* **76**, 1093 (2004).
29. T. Matozaki, Y. Murata, H. Okazawa, H. Ohnishi, *Trends Cell Biol.* **19**, 72 (2009).
30. C. M. Cameron, J. W. Barrett, M. Mann, A. Lucas, G. McFadden, *Virology* **337**, 55 (2005).
31. S. J. Stachelek *et al*., *Biomaterials* **32**, 4317 (2011).

Acknowledgments: The assistance of A. Secreto, J. Glover, and G. Danet-Desnoyers of the Stem Cell Xenograft Core at the University of Pennsylvania is very gratefully acknowledged as is technical assistance of K. Hsu, P. Bhoorasingh, and V. Carnevale. Support from the NIH (R01-EB007049, R01-HL062352, P01-DK032094, NCATS-8UL1TR000003, P30-DK090969) and NSF (Materials Research Science and Engineering Center, and Nano Science and Engineering Center-Nano Bio Interface Center) is also very gratefully acknowledged. P.L.R., D.A.P., and D.E.D. are authors on a patent applied for by the University of Pennsylvania on the Self peptide with first disclosure filed on 16 August 2010.

Supplementary Materials

www.sciencemag.org/cgi/content/full/339/6122/971/DC1
Materials and Methods
Figs. S1 to S10
Table S1
References (*32*–*44*)

31 August 2012; accepted 19 December 2012
10.1126/science.1229568

www.sciencemag.org/cgi/content/full/339/6122/971/DC1

Supplementary Materials for

Minimal "Self" Peptides That Inhibit Phagocytic Clearance and Enhance Delivery of Nanoparticles

Pia L. Rodriguez, Takamasa Harada, David A. Christian, Diego A. Pantano, Richard K. Tsai, Dennis E. Discher*

*To whom correspondence should be addressed. E-mail: discher@seas.upenn.edu

Published 22 February 2013, *Science* **339**, 971 (2013)
DOI: 10.1126/science.1229568

This PDF file includes

MATERIALS AND METHODS

Chemicals Streptavidin polystyrene beads were of different radius: 160nm, 1.1μm, 3.5μm, (Spherotech) and 100nm (Ademtech). Dulbecco's phosphate-buffered saline (DPBS) without Ca^{2+} or Mg^{2+} (Invitrogen) was supplemented with 1% BSA and 0.05% Tween 20 (Sigma-Aldrich). TBS (Tris-buffered saline) and TTBS (TBS with Tween 20) were used in Western blotting. Hoechst 33342 (Invitrogen, Carlsbad, CA) was used for DNA stains. RBC lysis Buffer (Roche Diagnostics Corporation) was used in Neutrophil isolation from NSG mice. The near-infrared lipophilic dye, DiR, and the deep red dye, DiD, were purchased from Invitrogen, Inc. and PKH26 Red Fluorescent Cell Linker Kit for General Cell Membrane Labeling from Sigma Aldrich. Chloroform, methanol, and hydrochloric acid were purchased from Fisher Scientific. N-Biotinyl-NH-$(PEG)_4$-COOH was purchased from EMD Chemicals, PEG Biotin, MW 550 was purchased from Nanocs Inc., and mPEG-Biotin, MW 5,000 from Laysan Bio Inc. Blebbistatin (±) was purchased from EMD Biosciences, and NSC-87877 was from Sigma.

Antibodies Fluorescein-labeled antibody anti-hCD47-FITC (clone B6H12, BD Biosciences) and anti-mCD47-FITC (clone mIAP301, BD Biosciences). Targeting to hCD47 used biotin anti-humanCD47 (BioLegend), and blocking mSIRPα was done with anti-CD172a (BD Biosciences). Quantification of hSIRPα used SE7C2 clone (Santa Cruz Biotech). To detect mouse macrophages, we used F4/80 antibody (clone 636, Santa Cruz Biotechnology). Opsonizing antibodies against mouse RBCs included rabbit anti-mouse RBC (Sigma-Aldrich); opsonizing antibodies against streptavidin coated polystyrene beads (Spherotech) included rabbit anti-streptavidin (Sigma-Aldrich) and rabbit anti-streptavidin conjugated with FITC (Rockland Immunochemicals) was used as IgG opsonin in phagocytosis assays. Antibody against nonmuscle myosin-IIA was obtained from Sigma-Aldrich. Secondary antibodies used for detecting opsonin levels and uningested beads included goat anti-rabbit FITC or goat anti-rabbit $F(ab')_2$ R-PE (Sigma-Aldrich). Secondary antibodies used for detecting soluble SIRPα or biotinylated CD47 binding included anti-GST Alexa 488 (Invitrogen) and Cy5 conjugated Affinity Purified Anti-Biotin goat (Rockland Immunochemicals), respectively. To measure the level of PEG molecules bound to streptavidin coated polystyrene beads we used Biotin-4–fluorescein (Anaspec).

Recombinant Proteins and hCD47 Peptides Recombinant human CD47 and soluble human SIRPα were made per (*16*). Human was the focus due to a lack of *in vivo* experiments on human-CD47 and known differences with mouse.

In considering synthesis of a 'Self'-peptide, mouse and human CD47 differ by about 40% in the sequence that binds SIRPα's N-terminal domain, and these differences include one or more amino acids in each of three distinct binding sequences in the co-crystal. 'Self'-Peptides were simulated for stability and interactions and then synthesized by standard solid phase methods in order to assess whether a synthetic, human-based ligand binds and signals to phagocyte receptors to passivate the innate immune cells responsible for clearing foreign objects of many forms. The peptides are:

(1a) 21 aa, >80% purity, Biotin-Acp (N-Term.) – GNYTCEVTELTREGETIIELK ('Self'-peptide)
(1b) 21 aa, >90% purity, Biotin-$dPEG_4$ (N-Term.) – GNYTCEVTELTREGETIIELK ('Self'-peptide)
(2) 12 aa, >80% purity, Biotin-Acp (N-Term.) – CEVTELTREGEC (disulfide 'Self'-SS-peptide)
(3) 10 aa, 10 mg, >90% purity, Biotin-$dPEG_4$ (N-Term.) – EVTELTREGE ('Self'-hairpin)
(4) 10 aa, 10 mg, >90% purity, Biotin-$dPEG_4$ (N-Term.) – EGERTLETVE ('Scrambled', i.e. reversed)
Acp denotes an aminohexanoic acid linker 'C6'.

mCD47 GNYTC EVTELsREGk TvIELK
human variants: GNYTC EVTELTREGE TI(I,T)ELK

SIRPα reverse transcriptase PCR and sequence The SIRPα variant expressed in THP-1 macrophages was determined after RNA extraction (Qiagen) using a one-step reverse transcriptase PCR (RT-PCR) amplification (Invitrogen). Samples of the PCR product were run on 1% agarose gel and gel purified for sequencing. Primers used for both RT-PCR and sequencing are: 5′-GGGTGAGGAGGAGCTGCAGGTGATT-3′ and 5′-GCGCTCGAGCCGTTCATTAGATCC -3′.

Plasmid construction for human-SIRPα and polymorphisms pEGFP-N1 plasmid with a CMV promoter (Clontech laboratories, Mountain View, CA) had the full extracellular domain of human SIRPα inserted using primers 5′-GCAGAGCTGGTTTAGTGAACCG-3′ and 5′-CGTCGCCGTCCAGCTCGACCAG-3′. Full-length human SIRPα variants v1-10 as denoted in (*14*) were generated through a series of point mutants in human-SIRPα variant 2, using the QuikChange Site-Directed Mutagenesis kit (Stratagene). All constructs were confirmed by sequencing. The following primers were used:
5′-CTGGAGAGACGGCCACTCTGCGCTGCACTGCGACCTCCC-3′ and
5′- GGGAGGTCGCAGTGCAGCGCAGAGTGGCCGTCTCTCCAG-3′
for mutations S54T, I56T, H58R, V61A;
5′-GAGGAGCTGGACCAGGCCGGGAATTAATCTA-3′ and
5′-TAGATTAATTCCCGGCCTGGTCCAGCTCCTC-3′ for mutations A79G;
5′-CACTTCCCCCGGGTAACAACTGTTTCAGATTTAACAAAGAGAGAAAACA-3′ and
5′-TGTTTTCTCTCTTTGTTAAATCTGAAACAGTTGTTACCCGGGGGAAGTG-3′ for mutations E99D;
5′- ATTCAGCCTGACAAGTCCGTATTAGTTGCAGCTGG-3′ and
5′-CCAGCTGCAACTAATACGGACTTGTCAGGCTGAAT-3′ for mutations S48L;
5′- GTTTCAGATTTAACAAAGAGAAATAACATGGACTTTTCCATCAGG-3′ and
5′-CCTGATGGAAAAGTCCATGTTATTTCTCTTTGTTAAATCTGAAAC-3′
for mutations E104N;
5′-CATGGACTTTTCCATCAGGATCGGTAACATCACCCCAGCAG-3′ and
5′-CTGCTGGGGTGATGTTACCGATCCTGATGGAAAAGTCCATG-3′
for mutations S111R, S113G;
5′-GGAAAGGGAGCCCTGACGTGGAGTTTAAGTCTGGAG-3′ and
5′-CTCCAGACTTAAACTCCACGTCAGGGCTCCCTTTCC-3′ for mutations T135V;
5′-GAAAGGGAGCCCTGACGACGTGGAGTTTAAGTCTGG-3′ and
5′-CCAGACTTAAACTCCACGTCGTCAGGGCTCCCTTTC-3′ for inserting D at 135.
hSIRPα variant 2 to 3 was constructed with the primers
5′- GTCGGCCATTCTGCTCTGCACTGTGACCT-3′ and
5′- AGGTCACAGTGCAGAGCAGAATGGCCGAC-3′ for mutations H58L.
hSIRPα variant 2 to 4 was constructed using primers:
5′-GCGGGTGAGGAGGGGCTGCAGGTGATT-3′ and
5′- AATCACCTGCAGCCCCTCCTCACCCGC-3′ for mutations E37G;
5′-TCTGCACTGCACTGCGACCTCCCTGATCC-3′ and
5′- GGATCAGGGAGGTCGCAGTGCAGTGCAGA-3′ for mutations V61A.
hSIRPα variant 2 to 7 was constructed using the following primers:
5′- CTGTCTGTGCGTGGCAAACCCTCTGCC-3′ and
5′- GGCAGAGGGTTTGCCACGCACAGACAG-3′ for mutations A149G.
hSIRPα variant 2 to 10 was constructed using primers
5′- TGCGCCTGGTCAAGAGTGGCGGGTG-3′ and
5′-CACCCGCCACTCTTGACCAGGCGCA-3′ for mutations G31R.
hSIRPα variant 1 to 5 was constructed using primers
5′- GGTGATTCAGCCTGACAAGTTCGTATTAGTTGCAG-3′ and
5′- CTGCAACTAATACGAACTTGTCAGGCTGAATCACC-3′ for mutations S46F.
hSIRPα variant 1 to 6 was constructed using primers:
5′- AGATTTAACAAAGAGAAATAACATGGACTTTCCCATCAGGATCGGTAA-3′ and
5′- TTACCGATCCTGATGGGAAAGTCCATGTTATTTCTCTTTGTTAAATCT-3′ for mutations S109P.
hSIRPα variant 1 to 9 was constructed using primers
5′- ACTTTTCCATCAGGATCAGTAACATCACCCCAGCA-3′ and
5′-TGCTGGGGTGATGTTACTGATCCTGATGGAAAAGT-3′.

Cell cultures and transfection COS-1, CHO-K1, A549, THP-1 cells (American Type Culture Collection) were respectively maintained in DMEM, MEMα, F-12, RPMI 1640, and DMEM low glucose media (Invitrogen) supplemented with 10% heat inactivated FBS (Sigma-Aldrich). Cells were detached for passaging using 0.25% Trypsin/0.5mM EDTA (Invitrogen). Differentiation of THP-1 cells was achieved in 100 ng/mL phorbol myristate acetate (PMA) (Sigma-Aldrich) for 2 days and confirmed by

attachment of these cells to tissue-culture plastic. Peripheral blood monocytes from human donors were obtained through the Human Immunology Core (Univ. Pennsylvania, School of Medicine). hSIRPα v1-10 were transfected into CHO-K1 cells with Lipofectamine 2000 (Invitrogen), and clones selected in 400 μg/ml G418 (Invitrogen). Expression of hSIRPα–GFP was confirmed by anti-SIRPα. Transfected cells were harvested using DPBS supplemented with 2 mM EDTA (Invitrogen) 1-2 days post-transfection for analysis of hCD47 binding.

Preparation of erythrocytes for injection Blood from NSG mice was acquired by cardiac puncture, and erythrocytes were separated from the rest of the blood components by a centrifugation gradient. Samples were divided into two groups, and labeled with either of the lipophilic dyes DiD or PKH 26 by co-incubation for 20 min at room temperature (RT). Both samples were washed with PBS/ 0.4% BSA and then one of them was incubated with anti-mCD47 (mIAP) primary antibody for 45 minutes and both of them were opsonized with excess rabbit anti-mRBC prior to mixing cells together and injecting into the tail vein for 30 min at RT. Cells were then washed with PBS/ 0.4% BSA and quantified by light and fluorescent microscopy

Preparation and characterizations of Nanobeads with CD47, 'Self' peptide, and Opsonin
Beads enable facile addition of 'Marker of Self' ligands, but rigid beads must be far smaller than highly flexible RBC to avoid first-pass clearance from the microcirculation (*39*). Nanoparticles are thus needed but if they are too small, then they can be a challenge to controllably modify and fully characterize after injection.

Streptavidin-coated polystyrene beads of 160 nm radius (SVP-03-10; Spherotech, Lake Forest, IL) were washed and blocked 3x in PBS plus 0.4% BSA. Manufacturer specifications of about $3x10^4$ Biotin–fluorescein sites per nanobead were confirmed by flow cytometry with fluorescence calibration beads and equate to about 1 biotin site per 10 sq.nm (Fig. S2A). This is the maximum density of modification (eg. PEGylation) achievable with these nanobeads, and compares well with useful densities in related contexts. Malmsten et al. reported 95% suppression of protein adsorption (at a specified time point) for PEG surfaces with 1 polymer per 10 sq.nm (*40*) although protein adsorption was still measurable. In addition, with liposomes the area per lipid is 0.7 sq.nm, and PEGylated liposomes exhibit 'stealth' in circulation with 2-5% PEGylation (eg. (*3*) main text), which equates to one PEG chain per 14 - 35 sq.nm.

Recombinant biotinylated hCD47 or synthetic biotinylated 'Self'-peptide were attached to the beads and then rabbit anti-Streptavidin conjugated with FITC was added as an opsonizing IgG-antibody (Rockland Immunochemicals). Beads were incubated at room temperature for 30 min, washed 3x, and re-suspended in PBS plus 0.4% BSA. The density of hCD47or 'Self' on the beads was determined by binding to soluble hSIRPα at 1 μM (see Binding Isotherms below) and, for hCD47, labeling with 15 μl of anti-hCD47-FITC (clone B6H12, BD Biosciences). Binding of hSIRPα was thus used to confirm similar levels of attachment of hCD47or 'Self' on the beads (see Fig. 3A). The opsonin density on the beads was determined with 1 μl goat anti-rabbit $F(ab')_2$ R-PE incubated for 30 min at room temperature. Beads were washed and resuspended in PBS for flow cytometry and further analyses.

Zeta potential measurements (Malvern Zetasizer) on key samples of Fig. 1C showed no significant differences: for (anti-streptavidin nanobeads), (hCD47 + anti-streptavidin nanobeads), ('Self'-peptide + anti-streptavidin nanobeads), (Scrambled peptide + anti-streptavidin nanobeads) all had a measured Zeta potential = -3.5 ± 1 mV. Sizes from light scattering for these nanobeads as well as PEGylated nanobeads conformed to manufacturer's specifications within about 10%. Forward and Side scatter in flow cytometry from pre-injected nanobeads provided additional evidence of uniformity of size even after the modifications.

Binding isotherms The binding isotherm of soluble hSIRPα was performed for 'Self'-peptides and full length hCD47 attached to the streptavidin polystyrene beads as noted over a range of concentrations using flow cytometry. Forward scatter, side scatter and fluorescence (FL1, FL2, FL3, FL4 channels in

logarithmic mode) were acquired for at least 10^4 events using a FACScan or FACSCalibur (BD Immunocytometry Systems). Data points from flow cytometry were plotted and fitted to obtain the K_d values as shown. A related analysis was used in the case of hCD47 binding to NSG monocytes and neutrophils. The K_d = 4 μM corresponds to an affinity within a 10-nm gap between membranes of about 40 molecules/(10 μm)^2, which differs from the K_i above by ~100-fold, as seen also in studies of THP1 cells (*14*). The difference suggests that almost all SIRPα that diffuses into the gap will bind and enrich in the synapse.

Measuring Beads and RBC in circulation The total number of beads remaining in circulation were measured using flow cytometry analysis of whole blood sampled from each mouse. Beads, in whole blood sample (or serum), were labeled with 15μl of anti-hCD47-FITC and with 1μl goat anti-rabbit F(ab')2 R-PE against the rabbit anti-streptavidin used as the opsonin for 30 min at room temperature. Beads were washed and resuspended in PBS for flow cytometry analysis of a 10ul sample. Forward scatter, side scatter and fluorescence (FL1, FL2, FL3, FL4 channels in logarithmic mode) were acquired using a FACScan or FACSCalibur (BD Immunocytometry Systems). From flow cytometry, the total number of beads was counted as the total number of events with the appropriately distinct forward and side scatter, and these events also appeared positive for the opsonin and hCD47.

Isolation of NSG neutrophils and monocytes Equal volumes of neutrophil isolation media and mice blood were added to a centrifuge tube and centrifuged at 500 RCF for 35 min. The blood is separated out into distinct components, including separate bands for monocytes and neutrophils. Carefully the layers of neutrophils and monocytes were isolated and placed into a tube with 10 mL of HBSS and centrifuged at 350 RCF for 10 minutes. The subsequent pellet contained neutrophils, monocytes, and residual red blood cells (RBCs). The supernatant was discarded and 2 mL of Red Cell Lysis Buffer was added to lyse the residual RBCs and centrifuged at 250 RCF for 5 min. The supernatant was removed and the pellet containing monocytes and neutrophils was resuspended in 250ul of PBS.

In vivo blocking of mSIRPα We blocked mouse-SIRPa within NSG mice by pre-injecting 100 μg anti(mouse-SIRPa) antibodies (anti-CD172a; BD Biosciences) that block binding of mouse-SIRPa to CD47 *in vitro*. Our results show (in inset to Fig. 3B) that when anti(mouse-SIRPa) is bound to splenic macrophages in the pre-injected mice, CD47 provides no advantage in circulation. In brief, the same CD47 particles as used in Fig. 3A were injected into 5 mice after pre-injecting anti(mouse-SIRPa) into 4 of the mice (30-120 min before). The Circulating Particle Ratio at 35 min was measured as in Fig.3A, and we also broke up the spleen and used flow cytometry to immunostain for macrophages (per Fig. 4A), of which 80% were positive for anti(mouse-SIRPa). Control mice that were not pre-injected with anti(mouse-SIRPa) were negative for anti(mouse-SIRPa).

Collagenase Digestion. Spleens were chopped into pieces and placed into tubes containing 1 ml of collagenase/DNase solution [1 mg/ml type II collagenase (Worthington Biochemicals) and 0.1% DNase I (Sigma) in RPMI medium 1640 plus 10% FBS]. The suspension was pipetted intermittently for 20-30 min at 37°C. Cells were then washed, treated to remove red blood cells, and counted before staining for flow cytometry to immunostain for macrophages with F4/80 (Bioscience, Inc.). Forward scatter, side scatter and fluorescence (FL1, FL2, FL3, FL4 channels in logarithmic mode) were acquired using a FACScan or FACSCalibur (BD Immunocytometry Systems).

Phagocytosis Assay For phagocytosis assays, macrophages were plated in 4cm2 or 2cm2 Lab-Tek II Chambered Coverglass (Nalge Nunc International) at 1.5 x 105/cm2. Streptavidin polystyrene beads were added to macrophages at a ratio of 2:1, 20:1, 277:1, and 2206:1 respectively and incubated at 37˚C for 45 min. The ratios were determined based on the surface area of the particles to normalize for particle size differences that resulted in comparable uptake among size ranges tested. Non-internalized beads were

washed away with PBS. Cells were fixed with 5% formaldehyde (Fisher Scientific) for 5 min, followed by immediate replacement with PBS. For differentiation of non-internalized beads, beads were labeled with a primary antibody, rabbit anti-streptavidin (Sigma-Aldrich) at 1:1,000 in PBS for 20 min at 25°C. A second antibody, anti-rabbit R-PE (Sigma-Aldrich) was added at 1:1000 in PBS to the cells and incubated for an additional 20 min at 25°C. Cells were then washed with PBS/ 0.4% BSA and then quantified by light and fluorescent microscopy. At least 200 cells were scored per well and experiments were repeated at least three times.Images were acquired with an inverted microscope (Olympus; IX71) with a 60x and 150x (oil, 1.4 NA) objective using a Cascade CCD camera (Photometrics, Tuscon, AZ). Image acquisition was performed with Image Pro software (Media Cybernetics, Silver Spring, MD). All subsequent image analysis was done using ImageJ.

For stimulated phagocytosis assays, beads with or without 'Self'-peptide, PEG or CD47 were incubated with rabbit anti-streptavidin as the opsonin. Beads were opsonized at the respective concentration for 30 min at RT. Opsonized beads were washed 2x and resuspended in 50 µl of PBS/0.4% BSA. Phagocytes were washed with PBS beads were labeled as described above.

For cytoskeletal involvement at the phagocytic synapse, streptavidin beads opsonized with rabbit anti-streptavidin FITC. Opsonized beads of different sizes were added to PMA treated THP-1 cells and immediately placed at 4°C for 10 min to synchronize phagocytosis. The temperature of the cells was then immediately increased to 37°C for 10 min and then fixed with 5% formaldehyde for immunofluorescence. For studies involving blebbistatin (EMD Biosciences), macrophages were treated for 10 min at 4ºC prior to temperature increase to 37ºC or for 45 min. Macrophages treated with DMSO were used to verify no solvent effects.

SHP-1 inhibitor effect on phagocytosis PMA activated THP-1 macrophage was treated with a SHP-1 inhibitor (NSC-87877) kindly provided by Dr. Frank L. Conlon (University of North Carolina) from 0-100 nM in DI water for 5 min prior to the addition of IgG-opsonized particles. Phagocytosis assay of IgG-opsonized particles coated with or without CD47 at 100 nm and 1.1 µm radius were conducted as described above.

Inhibition of nanoparticle uptake THP-1 macrophages activated with PMA were incubated with 10 µg/ml chlorpromazine in distilled water or 30 µM cytochalasin B in DMSO (Sigma-Aldrich) for 30 min at 37°C. Control cells were incubated with the medium with solvent. Followed by incubation with the above inhibitors, THP-1 cells were used for uptake studies with or without IgG-opsonized 100 nm radius particles targets as described above.

Immunofluorescence microscopy Immunostaining was performed after cells were fixed and blocked for 1 h with 5% BSA in PBS. Staining with primary antibody anti-rabbit PE-conjugated (1:200) was used for detection of non-phagocytosed beads for 1 h at room temperature in PBS. After washing, samples were fixed with 5% formaldehyde and imaged. In order to ensure that the cells were not permeable to labeling an antibody against myosin IIA was used to confirm no intracellular labeling occurred (Sigma-Aldrich). Images were acquired on an inverted microscope (IX71; Olympus) with a 40x or a 60× (oil, 1.4 NA) objective using a Cascade CCD camera (Photometrics). Image acquisition was performed with Image Pro software (Media Cybernetics, Inc.). All subsequent image analysis was done using ImageJ.

Immunoprecipitation and Western blotting Human Phagocytes, THP-1 wild-type ($2x10^6$) were cultured and differentiated in 6-well plates for 48 hours after PMA differentiation. Human CD47, PEG and Polypeptides were attached to 2.1µm diameter beads at specific densities as described above and added at a bead to cell ratio of 20:1 for 10 minutes. Following the incubation time, the cells were washed with ice-cold PBS and then lysed on ice in 300 µl of lysis buffer (50 mM Tris-HCl (pH 7.4), 150 mM NaCl, 1mM EDTA, 1% NP-40, 1% protease inhibitor cocktail [Sigma-Aldrich] and 2mM activated sodium orthovanadate). For immunoprecipitation, whole lysate was mixed with 1:200 anti-SIRPα

(SE7C2) antibody (Santa Cruz Biotechnology, Inc.) with Protein G agarose (Pierce) at 4˚C overnight. Precipitated proteins were placed in 4-12% SDS-PAGE in MOPS buffer (Invitrogen), transferred to PVDF membrane, blocked and labeled via phosphotryosine IgG HRP-conjugated (Cell Signaling) and anti-SIRPα (C-20) (Santa Cruz Biotechnology, Inc.) as primary antibodies and anti-goat-HRP (Amersham). All Westerns were run in duplicate, along with an additional blot for actin to ensure constant protein load among samples.

Biodistribution Study with dye-labeled Beads All mice were treated in accordance with approved IACUC protocols at the University of Pennsylvania. Near Infrared Fluorophore (NIRF)-labeled and unlabeled streptavidin coated polystyrene beads (~10^7 in 50 mL PBS) were injected into the tail veins of healthy adult Immune-deficient (NSG) Mice (4-8 weeks). Some variability in injected bead number is due to variability in locating the tail vein, but the two-color ratio method readily accounts for such variability. Every 10 min, 50μl blood samples were collected by retro-orbital bleeding. At 35 min following injection, mice were sacrificed and whole blood, liver, spleen, lungs, kidneys, heart and brain were collected. The whole blood was then centrifuged and plasma collected.

Organs were imaged on the LiCor Odyssey imaging system (LI-COR Biosciences, Lincoln, NE) at 800 nm excitation. The integrated fluorescence intensity of the organs was normalized using the organ correction factor found by Christian et. al. (*41*) and applied to all other measured intensities for all organs. The NIR intensity of the plasma was measured on the LiCor and calculated by fitting the slope of the linear dilution curve. Although biodistribution analyses showed that hCD47-nanobeads gave significantly lower signals in spleen and higher signals in blood, spleen and liver still dominate analyses of isolated tissues as in many other studies using a variety of materials.

The fraction of total blood in the tumor must be estimated in order to determine the % of injected nanobeads within the Tumor blood (Fig. 2C, inset). The typical tumor weight is about 500 mg, which we approximate as 1 g, and assume the tumor has 10% blood volume like other highly vascularized tissues such as liver and spleen (*42*). One measurement reported tumors are ~2% blood by volume (*43*), so the assume values of 10% and 1 g provide an overestimation of the amount of NIR intensity in the tumor provided by NIRF-labeled particles in the blood. This overestimation allows us to safely determine that particles functionalized with 'Self'-peptide or hCD47 have entered the tumor stroma.

Paclitaxel loading, MTT Assay, Body Weight, and Tumor Size Polystyrene beads (10^8) were suspended in 300 μL Milli-Q water. 5 μL of 4.5 mg/mL paclitaxel (LC Laboratories) in methanol was added to the beads to achieve 75 μg/mL concentration. After overnight incubation at room temperature and following spin-down, beads were re-suspended in PBS with 10-fold concentration. The beads were then modified by attaching 'Self' peptides, etc..

For MTT assay, 5000 A549 cells were seeded on wells of 96-well plate, 24 hours prior to drug treatment. Cells were treated with series dilution of beads samples loaded with paclitaxel, starting from 7.5 μg/mL. After 24 hours incubation at 37°C with 5% CO_2, cells were washed once with PBS and added with 100 μL growth medium and 20 μL of 5 mg/mL Thyazolyl Blue Tetrazolium Bromide (Sigma). After 4 hours incubation at 37°C with 5% CO_2, purple crystal in the cells were solubilized by adding 100 μL DMSO. Absorbance was read at 560 nm.

To assess safety of formulations, healthy NSG mice received intravenous (i.v.) injections of paclitaxel-loaded beads or Cremophor EL (Sigma) all at an equal dose of 7.5 mg/kg. Body weight of each mouse was measured right before and 24 hours after the injection, and by convention an excessive dose would be defined by more than 10% loss in body weight in 24 hrs.

To assess efficacy of formulations, cancer cells were injected subcutaneously about 6 weeks before treatment. Tumor-bearing mice were then treated with daily i.v. injections of paclitaxel-loaded beads at a dose of 7.5 mg/kg. Tumor size was measured daily, giving an estimation of volume with Tumor volume = ½ (major axis) * (minor axis)^2 (*44*). As a positive control for tumor shrinkage, paclitaxel solubilized with Cremophor was injected at 22 mg/kg (*33*).

Cryo sectioning and immunostaining Immediately after Licor whole-organ imaging, excised tumors were suspended in OCT medium (Sakura Tissue Tek) and frozen in liquid nitrogen. Frozen tumor tissues were sectioned on a Leica cryostat microtome (5 μm sections). A glass grid with numbered 500 μm squares (Electron Microscopy Sciences) was super-glued to the bottom of the slides under the tissue for reference. Phosphate buffered saline (PBS) with 1 μg/ml Hoechst trichloride trihydrate was added to rehydrate the tissue and visualize the nuclei. Samples were fixed in 3.7% Formaldehyde in PBS for 10 min, and permeabilized with 0.5% Triton-X100 for 10min. Samples were blocked with 10% BSA for 30 min and stained with the human-specific antibody F4/80 (Santa Cruz Biotechnology clone 636) at 1:100 in blocking solution, and stained at 1:300 with anti-rabbit R-PE (Sigma) conjugated secondary antibody for 1 h. After washing, samples were mounted with GelMount (Biomeda) and the same regions were reimaged using the grid as reference. Images were taken in Light and fluorescent microscopy at 60X magnification.

Biodistribution Study with Two Color-labeled Beads in Tumor-bearing NSG Mice Human lung derived carcinoma A549 cells (10^6) were suspended in PBS with 25% Matrigel (BD Bioscience) and injected subcutaneously into flank sites of each NSG mouse. After about 5 weeks, the tumor-bearing mice received tail vein injections of the 1:1 mixture of DiD and DiR dye-coated beads. Fluorescent intensity from both dyes in tumor areas was monitored at 10min, 40min, 90min and 120min, using Xenogen IVIS Spectrum Imaging System (Caliper Life Sciences, Hopkinton, MA). After 120 min post-injection, the mice were sacrificed for harvesting tumors as well as organs (liver, spleen, lungs, kidneys, heart, brain). Intensity from collected tissue was also acquired. Image analysis was done with Living Image Software (Cliper Life Sciences). All harvested organs and tumors were imaged with the LICOR Odyssey imaging system to measure accumulation of NIRF-labeled beads. These ex vivo studies remove background from nearby tissue and minimize any uncertainty in the region-of-interest compared to in vivo imaging.

Statistical Analyses All data unless noted are mean ±SEM, with *P* values obtained from *t* tests.

LEGENDS for SUPPLEMENTAL FIGURES and TABLES

Fig. S1. Two-color RBC experiment show for each color that mouse-CD47 prolongs Circulation, and Single Color Nanobead experiments also shows hCD47 and 'Self' peptide prolong Circulation.

(**A**) Schematic of competitive circulation and clearance in which two colors of nanobeads (or cells) are mixed and injected (50 μL in PBS) into the same mouse after labeling with either red (PKH26) or a far-red (DiD) fluorophores. The lower left plot illustrates that two different beads are cleared from the circulation of the same mouse at different rates; if both clearance processes fit exponentials as suggested, then their ratio is also exponential with a simple relationship between the decay constants (*A, B*) and the doubling time (*T*). Evidence of these functional forms is provided in Fig.1 (B and C) and this figure (B) and (D). (**B**) Representative images of blood samples taken at 10 min after injection of NSG mouse-RBC (mRBC) treated with anti-CD47 antibody (blue) or unblocked control mRBC (green). The opsonization level of the RBC was measured for each condition before injection, which showed approximately 2000 molecules/um^2 for both samples. Two-color RBC experiment shows that mouse-CD47 prolongs circulation independent of fluorescence labeling. 50 μl of blood was periodically sampled, and flow cytometry analysis of the decays in particle numbers were used to calculate the circulation kinetics for each condition in each mouse. A doubling time similar to that in Fig. 1B can be estimated from these results, and if it were extrapolated to one full day would yield $2^{24h/33min}$ (~10-trillion) more RBC with CD47 compared to every circulating *RBC without CD47*. This exceeds by ~100-fold the daily production of RBCs in humans and begins to suggest the potency of CD47 and/or co-factors on RBC. (**C**) Nanobeads in whole blood samples were identified using a unique methodology in flow cytometry for nanobeads in circulation. Forward and side scatter were used to separate nanoparticles from the rest of the blood components as well as by using anti-streptavidin antibody and the appropriate isotype controls (histograms) (**D**) Any Targeting antibody will also opsonize nanoparticles and promote *in vivo* clearance. Since CD47 has been therapeutically targeted with antibodies (*27*), we attached biotinylated-(anti-hCD47) (see Methods) to the nanobeads and co-injected in mice with beads having anti-streptavidin (n = 3 mice). Periodic bleeds were analyzed by flow cytometry with quantitation of 100-1000 particles and verification of antibody attachment to the nanobeads. Beads are cleared equally for both antibodies. (**E**) Single color nanobead studies show hCD47 and 'Self' peptide prolong circulation. 50 μl of blood was periodically sampled from mice injected with one type of functionalized bead (hCD47, 'Self' peptide, or IgG control), and the circulation kinetics of the beads was measured by flow cytometry.

Bare 320nm beads were cleared *in vivo* slower than IgG-opsonized but faster than beads functionalized with Opsonin+hCD47 and Opsonin+'Self' peptide. All data are means ±SEM.

Fig. S2. PEGylation of nanobeads can be in a 'stealthy' range, but pre-opsonized beads are efficiently phagocytosed *in vitro* and rapidly cleared *in vivo*, whereas PEG-beads without pre-opsonization circulate for hours with hCD47 enhancing the circulation. (**A**) Flow cytometry measurements of PEG-biotin density on nanobeads based on the number of fluorescein-biotin molecules bound subsequently to the nanobeads. Nanobeads with PEG densities > 0.6 chains per 10 sq.nm were used in subsequent studies and correspond to densities common with, for example, stealth liposomes [e.g., (*1-3*) main text]. (**B**) *In vitro* phagocytosis of opsonized PEG-nanobeads is efficient and independent of PEGylation, but phagocytosis is significantly inhibited by attachment of hCD47. See Methods and Fig. 4 for details of assay. (**C**) *In vivo* circulation studies of PEGylation similar to Fig. 1C with anti-streptavidin opsonized nanobeads plus biotinylated-PEG4 (n = 2), -PEG 0.5K (n = 2), or -PEG 5K (n = 1). Circulation appears statistically independent of PEG choice. (**D**) Single color nanobeads in circulation studies similar to Fig. S1E. PEG-beads without pre-opsonization circulate for hours longer than IgG-opsonized control nanobeads, but hCD47 + PEG significantly increases circulating nanobead number (n = 3; ±SEM). However, biotin-hCD47 is slowly lost in circulation as shown in Fig. 3A and Fig. S3E, and so the increase with hCD47 is likely to be underestimated. All data are means ±SEM.

Fig. S3. Human and Mouse CD47 inhibit Splenic clearance based on imaging the Spleen. (**A**) Human CD47 inhibits splenic clearance of highly opsonized (6000 molecules/μm^2) nanobeads in NSG mice. Accumulation of NIR-labeled nanobeads in the spleen was determined by total splenic NIR fluorescence intensity as measured by an Odyssey imaging system (LI-COR Biosciences) (**B**) Flow cytometry data shows binding of soluble mouse-SIRPα-GST to recombinant mouse CD47 attached to particles and also to nanoparticles with blocked mouseCD47 (mIAP301). Beads in circulation were collected 30 and 60 minutes after injection, and the concentration of beads opsonized with anti-streptavidin was compared to opsonized beads also coated with biotinylated mouse CD47. Spleens were harvested at 60 min after injection (n=3) and the number of particles were measured by splenic NIR fluorescence intensity (**C**) At 40 min post-injection of two colors of nanobeads, mice were sacrificed and whole blood, liver, spleen, lungs, kidneys, heart and brain were collected. NIR fluorescence intensity of each organ was measured and normalized for organ weight and optical density as well as for NIR signal resulting from particles in the blood volume of each organ. The NIR fluorescence intensity of the plasma was calculated by serial

dilution in PBS. Plot showed results for n = 6 animals per group of control 160 nm polystyrene opsonized beads (blue bar) and similar beads functionalized with biotinylated hCD47 (red bar). All error bars are SEM, and (*) indicates $p < 0.05$. For Scrambled-peptide, measurements were more limited but clearly show rapid clearance from blood. (**D**) Normalized NIR fluorescence intensity for all organs in tumor-bearing mice measured by the Odyssey imaging system (n=2). All data are means ±SEM.

Fig. S4. Tumor imaging with nanobeads is consistently enhanced by hCD47 and 'Self' peptide.(**A**) Tumor imaging is enhanced after second injection of hCD47-Nanobeads at 120 min after first injection. (**B**) Calibration of fluorescence emission and number of beads using a Xenogen IVIS Spectrum Imaging System (Caliper Life Sciences, Hopkinton, MA). (**C**) Tumors were excised from one set of tumor-bearing mice for *ex vivo* quantification by an Odyssey imaging system (LI-COR Biosciences). For control, N = 2; for 'Self' peptide, N = 4; and for hCD47, N = 6 tumors. Inset bargraph shows the high percentage of 'Self' nanobeads in the tumor compared to an upper bound (see Methods) for the nanobeads in the blood vessels within the tumors (N = 2). Scrambled peptide shows very little accumulation in the tumors or tumor vasculature (N = 2). All data are mean ±SEM.

Fig. S5. 'Self' nanobeads enhance efficacy of an anti-cancer drug *in vivo*. (**A**) *In vitro* viability of A549 human lung cancer derived cells in the presence of various formulations with Paclitaxel (Tax), which is a common anti-cancer drug in wide clinical use against solid tumors including lung tumors. Cremophore is a standard clinical carrier of Tax. Nanobeads of the four rightmost panels are, clockwise: IgG control with anti-Streptavidin, IgG plus biotin-hCD47 per Figs. 1C and 2, PEG-biotin, and biotin-(anti-hCD47) (without anti-Streptavidin). Cell viability was measured by standard MTT assay to determine the 50% inhibition constant (IC50). (**B**) Targeting of A549 cells with biotin-(anti-hCD47). Upper panel shows the cancer cells by forward/side scatter, lower left panel shows non-specific binding of the secondary Ab Cy5-anti-Biotin, and the lower right panel shows the specific binding between cells and biotin-(anti-hCD47). (**C**) Tumor sizes 4 days after daily injections and normalized to initial A549 tumors. Control Tax-nanobeads have anti-Streptavidin IgG (per Figs. 1C and 2) and hCD47 Tax-nanobeads also have this IgG; all beads were injected at the maximum drug load of 7.5 mg/kg Tax, whereas Tax-Cremophore was injected at 22 mg/kg. None of the drug treatments showed significant shrinkage until day 4. Tumor sizes were measured daily. (n ≥ 3 mice; ±SEM). (**D**) Small-molecule therapeutics are increasingly being combined with targeting antibodies, and we hypothesized that adding Self-peptide would provide further advantage. Tumor sizes were measured 1 day after a single injection of targeted Control Tax-nanobeads (anti-hCD47 IgG + PEG) or targeted Self-peptide Tax-nanobeads (Self-pept. + anti-hCD47 IgG + PEG).

CD47 is considered a therapeutic target on cancer cells [(*26)* in text], and chemotherapeutics are increasingly being combined with therapeutic antibodies as here. Note that Tax-Cremophore has no significant effect at day-1, whereas Self-peptide effectively shrinks the tumors. ($n \geq 3$ mice; ±SEM). The upper inset shows soluble hSIRPα binding to Self-peptide on beads with anti-hCD47, which indicates that anti-hCD47 does not inhibit Self-peptide activity. (**E**) *In vivo* safety of 7.5 mg/kg Tax was assessed by measuring body weight changes 24 hr after injection ($n = 3$ mice each). All mice showed <10% body weight loss, which is the conventional maximum for a tolerable dose, but Tax-Cremophore alone gave a statistically significant loss of body weight. (**F**) As part of efficacy studies at a higher therapeutic dose of 22 mg/kg Tax-Cremophore (*33*), visibly necrotic tails near the site of injection (images) were evident in 2 of 3 mice injected with Tax-Cremophore, with 1 mouse requiring amputation of the tail based on standard of care criteria. Cremophor is well known to cause allergic reactions, but the higher dose was otherwise tolerated with weight losses <10% body weight. The hCD47 tax-nanobeads showed no significant loss of body weight and no tail necrosis. All data are means ±SEM.

Fig. S6. CD47 is progressively lost from Nanobeads in circulation, and Nanobead Numbers at early times *do not* correlate with Bead Ratios at endpoint. (**A**) Increased surface density of hCD47 on the Nanobeads enhances the number of Nanobeads in circulation in single color bead experiments. Circulating Beads Numbers are proportional to the hCD47 concentration found on the surfaces of the beads measured by flow cytometry. Blood samples were taken at 10, 21 and 35 min after single color beads injections. (**B**) In two color bead experiments, the number of beads at early timepoints does not correlate with the ratio at 35 min. In other words, PEG and Scrambled peptide fail to enhance persistence in circulation over a broad range of particle numbers, while 'Self' and hCD47 do work over a broad range of particle numbers but otherwise show no trend. These results suggest that the macrophages are not saturated by the beads in these experiments; if the macrophages were saturated, then the likely trend would be a decay in hCD47 beads toward a ratio of 1 because control beads would no longer be cleared. Dashed lines indicates means.

Fig. S7. hSIRPα variants exhibit different affinities for hCD47. (**A**) GFP-tagged full-length human SIRPα GFP (hSIRPα-GFP) was confirmed to be transiently expressed in CHO-K1 cells by GFP expression, and surface expression was confirmed with anti-SIRPα antibody by flow cytometry. (**B**) Affinities of surface-expressed hSIRPα variant 10 for soluble hCD47 was measured by flow cytometry. Saturation binding fits gave the indicated dissociation constants, K_d. (**C**) Human SIRPα polymorphisms variants 1-9 expressed on

CHO cells with affinity binding to soluble hCD47 was based on flow cytometry. Saturation binding fits yield the dissociation constant, K_d was summarized in the plot with binding curves repeated in triplicate ± standard deviation. (**D**) The binding affinity of hCD47 bound to the surface of beads to hSIRPα was measured using varying concentrations of soluble hSIRPα v10 to determine the dissociation constant, K_d. (**E**) Linear relationship between the K_d obtained for surface-expressed hSIRPα polymorphisms variants 2,7 and 10 and soluble hCD47 and K_d obtained for hCD47 attached to beads and soluble hSIRPα variants. All data are means ±SEM.

Fig. S8. Molecular Dynamics Simulations of Structures reveal Folding and Interactions. (**A**) Full atomistic molecular dynamics (MD) simulations were performed for over 50 ns with the hCD47-hSIRPα complex (PDB: 2JJS), with each component in water at the indicated solution conditions in constant particle isothermal-isobaric ensemble (NPT) constraints. Systems were equilibrated for over 5 ns followed by production runs for structural analysis. The co-crystal structure of hCD47 and hSIRPα (*22*) identified the FG loop in hCD47 as one of two interaction sites, and so it formed the basis for design and simulation of several polypeptides. (**B**) The 'Self' peptide has interstrand hydrogen bonds that increase the stability of the hairpin, while the 'Self'-SS-peptide has a mutation at T107C that promotes a disulfide bridge with C96 and induces a torque and splay in the circularized peptide. Both peptide structures are stable since unstable configurations tend to rearrange within 10 ns (*34*). For electrostatic calculations of Fig. 3D we used Adaptive Poisson-Boltzmann Solver (APBS) (*35*) as implemented in VMD (*36*). (**C**) Peptide complexes with hSIRPα were obtained via computational docking. Structural heterogeneity of the peptide was taken into account by sampling of 100 representative configurations from a 100 ns long MD trajectory. Docking was performed using HADDOCK (*37*), an algorithm able to bias the stochastic exploration of the configurational space via aptly defined distance restraints between sets of residues from the two complex constituents. The configurational space of the complex was sampled via a three-stage protocol: (i) Randomization of orientations and rigid body energy minimization; (ii) Semi-flexible simulated annealing in torsion angle space; (iii) Final refinement by MD simulations in Cartesian space with explicit solvent. For each conformation of the peptide, 2,000 structures of the complex were generated, and from these the best 200 were employed for further analysis. Salt bridges of Fig. 3E were calculated by identifying pairs of negatively and positively charged atoms within 4 Å, (*38*) without accounting for relative orientation. (**D**) The upper right plot shows loop dimensions (as Root-Mean-Squared Deviation) versus time in solution for hCD47, for the 'Self' peptide, and for the disulfide containing 'Self'-SS-peptide, which tends to be larger (regime *c*). The lower histograms show the

frequency of salt bridges formed between these two peptides and hSIRPα when docking various configurations from the size ranges *a-c*.

Fig. S9. The role of particle size, Myosin IIA, and SHP-1 in particle phagocytosis by macrophages.

(**A**) Nano to micron sized IgG-opsonized particles can be observed in phase contrast images (top) and fluorescent microscopy (bottom) to determine phagocytosed (green) versus non-phagocytosed particles (yellow) (*see materials and methods*). The number of IgG-opsonized particles per phagocyte was plotted for 160 nm and 1.1 μm at either a constant particle surface area or constant particle number, with 200 phagocytes counted (n=3, ± SD). (**B**) In the presences of bacteria, THP-1 phagocytes (which display hSIRPα(v1)) that express: (i) wild-type GFP-Myosin IIA (MYH9) show localization with arrows indicating points of contact in phase contrast and GFP image insets. (ii) A tyrosine mutation of GFP-MYH9 results in non-functional MyH9 and thus no GFP localization in the presence of bacteria. (iii) In THP-1 macrophages expressing wild-type GFP-MYH9, GFP signal localizes around 1.1 μm particles alone. (iv) hCD47 attached to the particle surface inhibits GFP-MYH9 localization around the particles (v) Larger 3.4 μm particles show GFP-MYH9 localization (inset). Scale bar 10 μm (vi) hRBC provide a hCD47 control for GFP-MYH9 localization in THP-1 cells. (**C**) Streptavidin beads were coated with varying concentrations of biotinylated hCD47 and anti-streptavidin IgG as the opsonin. Inhibition of phagocytosis is dependent on the density of human CD47 on beads but independent of particle sizes ranging from 100 nm to 3.5 μm. Phagocytosis inhibition occurs with an effective $K_i \approx 20$ molecules/μm^2 for particles from micro to nano-meter beads. The vertical blue bar is the normal density of CD47 found on normal human RBC (~250 CD47/μm^2) and the horizontal gray bar indicates the level of phagocytosis of unopsonized beads. (**D**) IgG-opsonized particles of radius 100 nm or 1.0 μm with or without hCD47 on the surface were incubated with THP-1 macrophages with an SHP-1 Inhibitor (NSC-87877) at 62.5 nM. The effects of SHP-1 inhibition were determined by the ratio of ingested particles per THP-1 phagocyte (*see Materials and Methods*). The number of particles ingested are shown based on 200 phagocytes counted ($n \geq 3$, ± SD). Inset shows the concentration dependence of NSC-87877 effect on particle uptake. All data are mean ±SEM unless indicated.

Fig. S10. Phagocytic activation can be passivated almost independent of curvature through signaling by hCD47 and a minimal 'Self' peptide designed from the binding site with SIRPα.

Figure S1

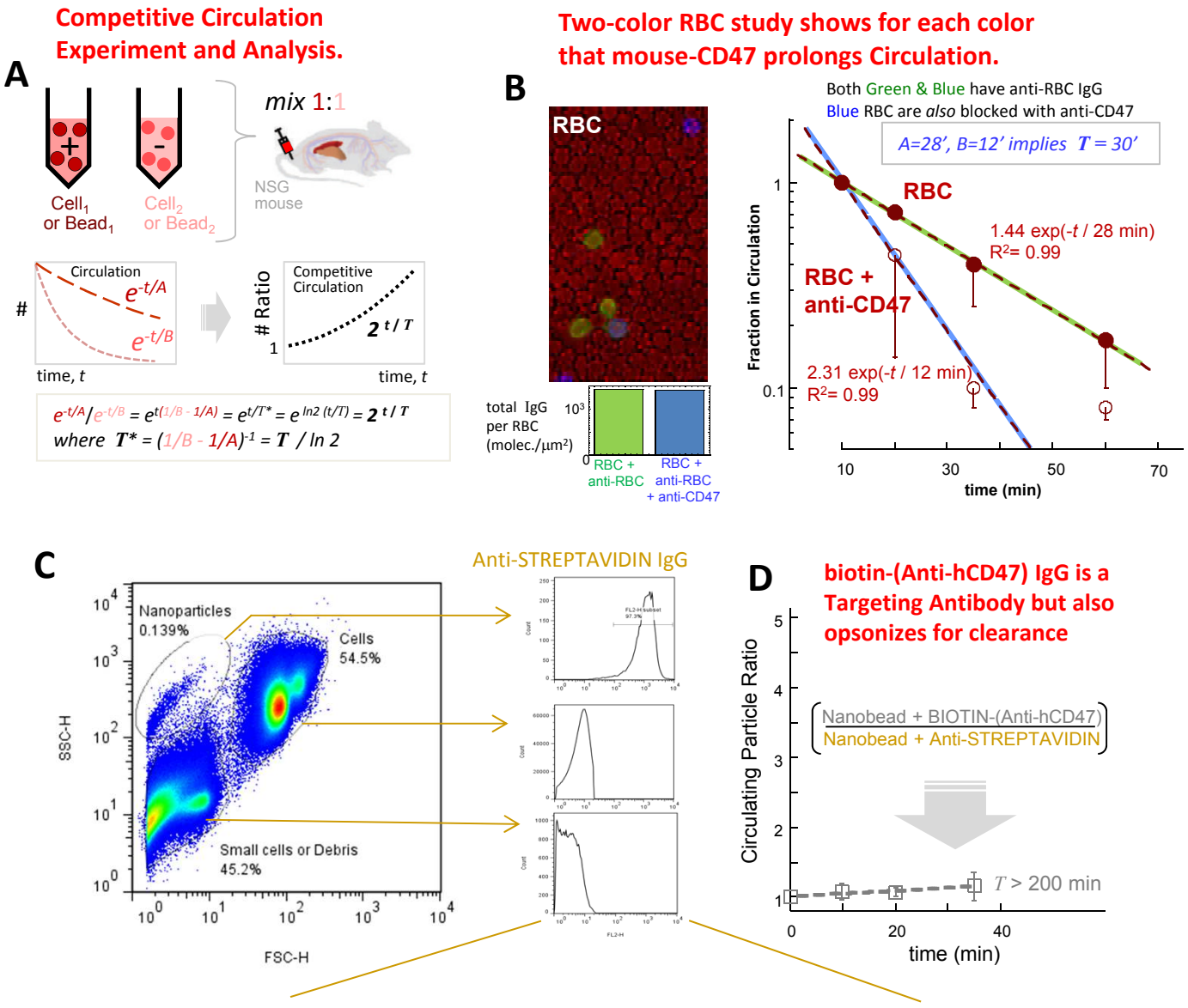
A
Competitive Circulation Experiment and Analysis.
mix 1:1
Cell1 or Bead1
Cell2 or Bead2
NSG mouse
Circulation
e-t/A
e-t/B
#
time, t
Ratio
Competitive Circulation
2 t / T
1
time, t
e-t/A / e-t/B = et(1/B - 1/A) = et/T* = e ln2 (t/T) = 2 t / T
where T* = (1/B - 1/A)-1 = T / ln 2
B
Two-color RBC study shows for each color that mouse-CD47 prolongs Circulation.
RBC
total IgG per RBC (molec./μm²)
10³
0
RBC + anti-RBC
RBC + anti-RBC + anti-CD47
Both Green & Blue have anti-RBC IgG
Blue RBC are also blocked with anti-CD47
A=28', B=12' implies T = 30'
RBC
1.44 exp(-t / 28 min)
R²= 0.99
RBC + anti-CD47
2.31 exp(-t / 12 min)
R²= 0.99
Fraction in Circulation
1
0.1
10
30
50
70
time (min)
C
Anti-STREPTAVIDIN IgG
Nanoparticles 0.139%
Cells 54.5%
Small cells or Debris 45.2%
SSC-H
FSC-H
D
biotin-(Anti-hCD47) IgG is a Targeting Antibody but also opsonizes for clearance
Nanobead + BIOTIN-(Anti-hCD47)
Nanobead + Anti-STREPTAVIDIN
T > 200 min
Circulating Particle Ratio
0
20
40
time (min)
E
Single Color Nanobeads experiments show hCD47 and 'Self'-peptide prolong Circulation even when there is no competition.
A=26', B=12' implies T = 31'
+hCD47
1.42 exp(-t / 26 min)
R²= 0.97
+'Self' peptide
1.32 exp(-t / 27 min)
R²= 0.90
IgG
2.15 exp(-t / 12 min)
R²= 0.98
Fraction of Nanobeads in Circulation
time (min)
Bare
1.62 exp(-t / 22 min)
R²= 0.98
IgG
2.15 exp(-t / 12 min)
R²= 0.98

Figure S2

PEGylation of nanobeads can be in a 'stealthy' range, but pre-opsonized beads are efficiently phagocytosed *in vitro* and rapidly cleared *in vivo*. Without pre-opsonization, PEG-beads circulate for hrs, and hCD47 enhances circulation.

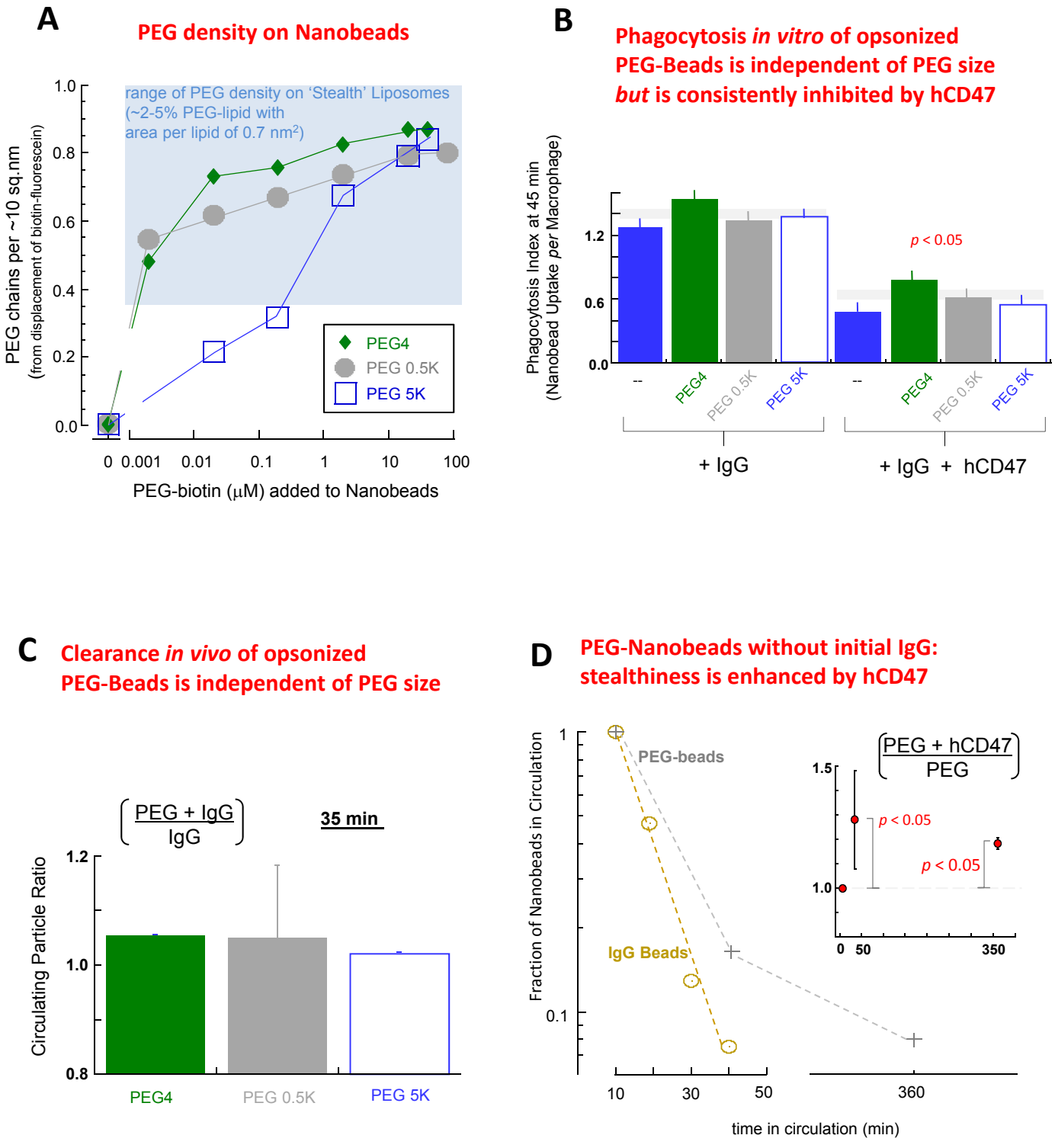

Figure S3

Human and Mouse CD47 inhibit Splenic clearance based on imaging the Spleen

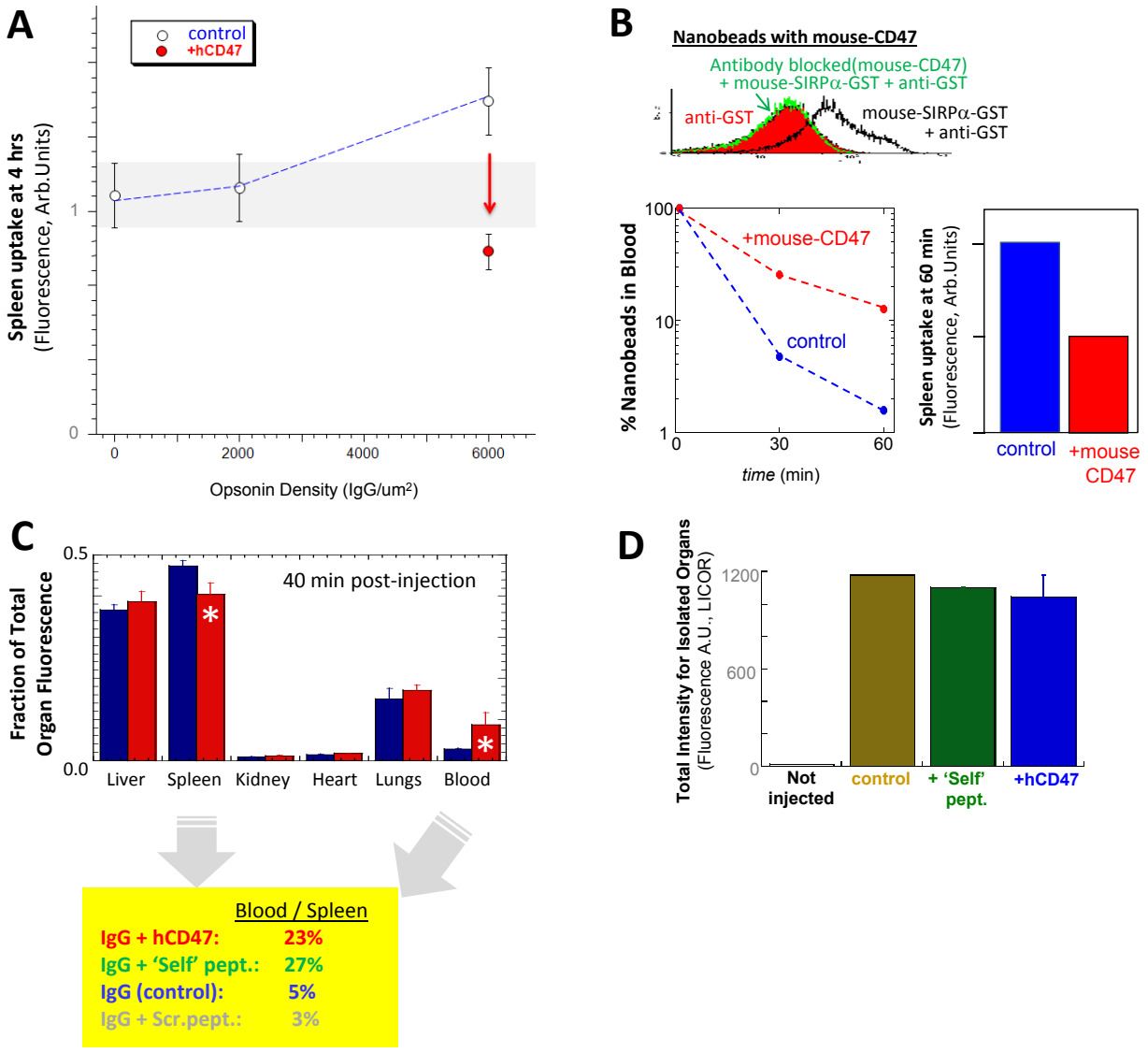

Figure S4

Tumor imaging with nanobeads is consistently enhanced by hCD47 and 'Self' peptide

Tumor imaging is enhanced after second injection of hCD47-Nanobeads

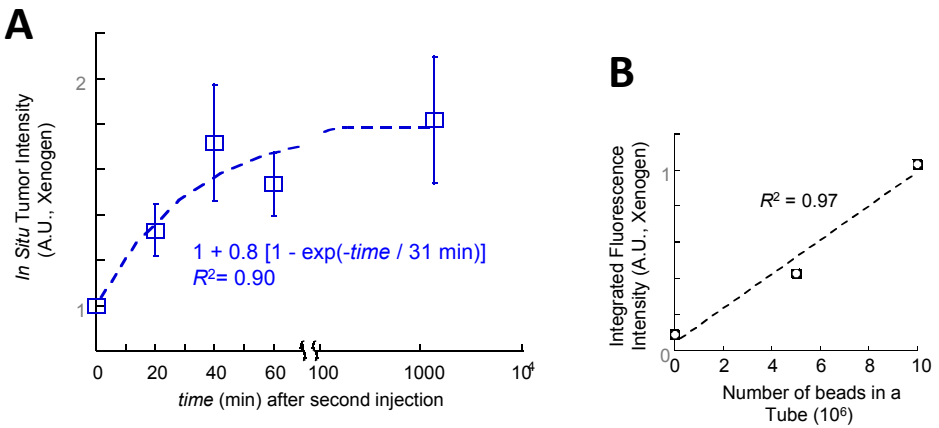

Excised Tumors confirm in vivo imaging and suggest beads leak into Tumors

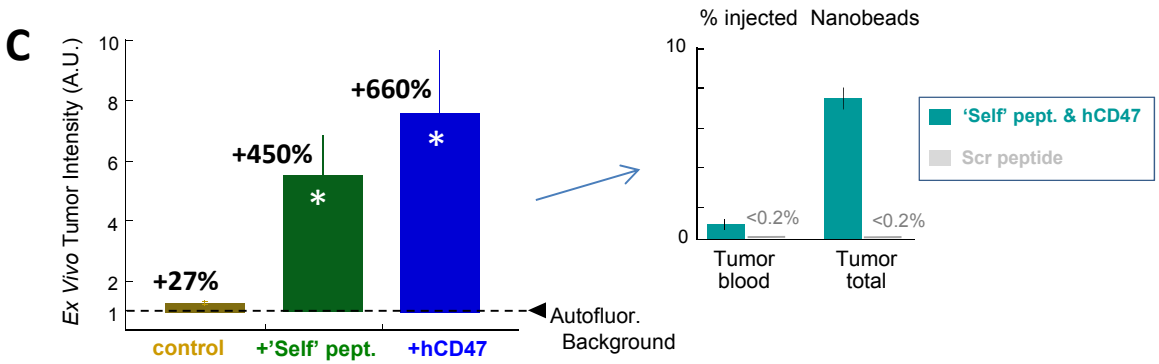

Figure S5

'Self' nanobeads enhance efficacy of an anti-cancer drug *in vivo.*

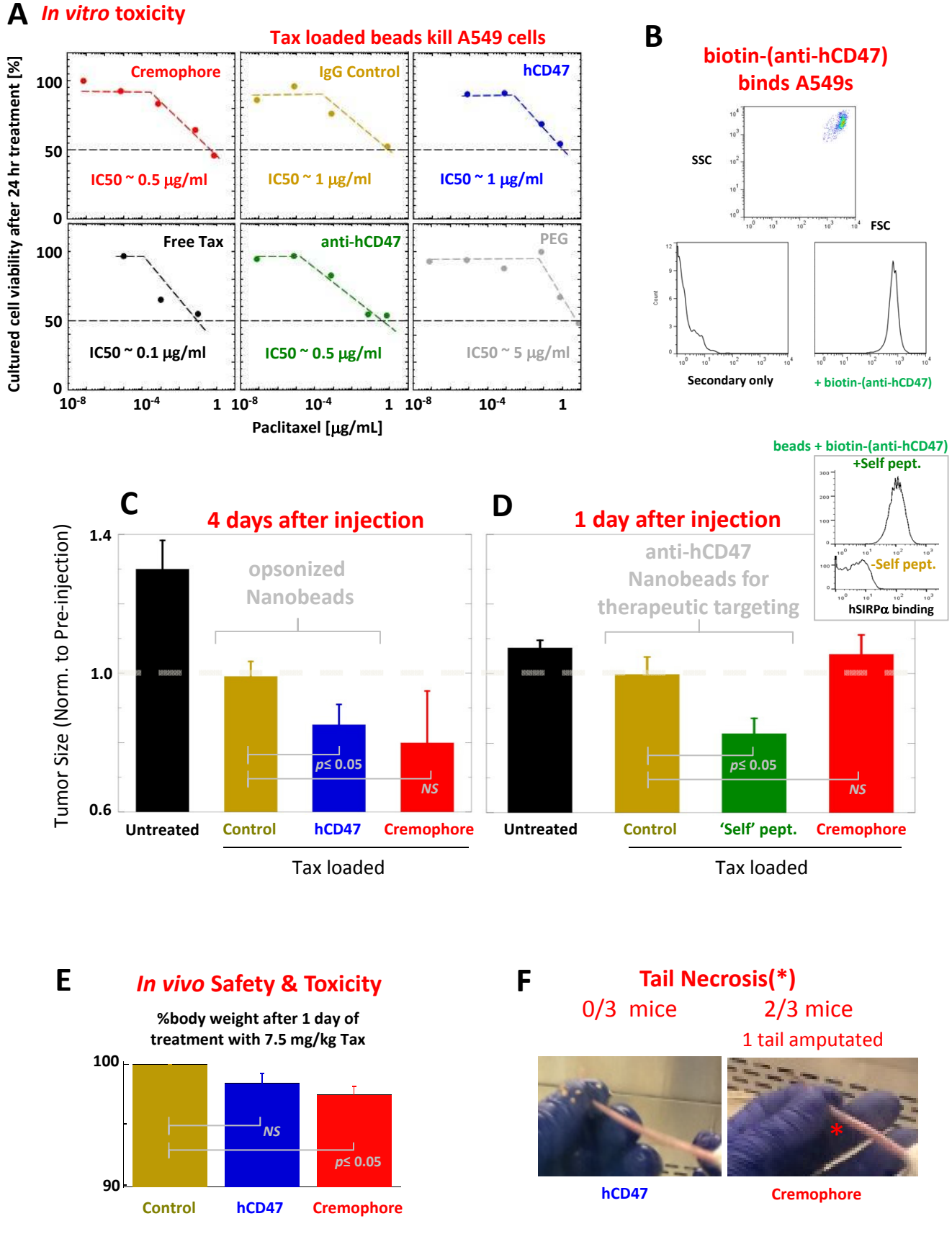

Figure S6

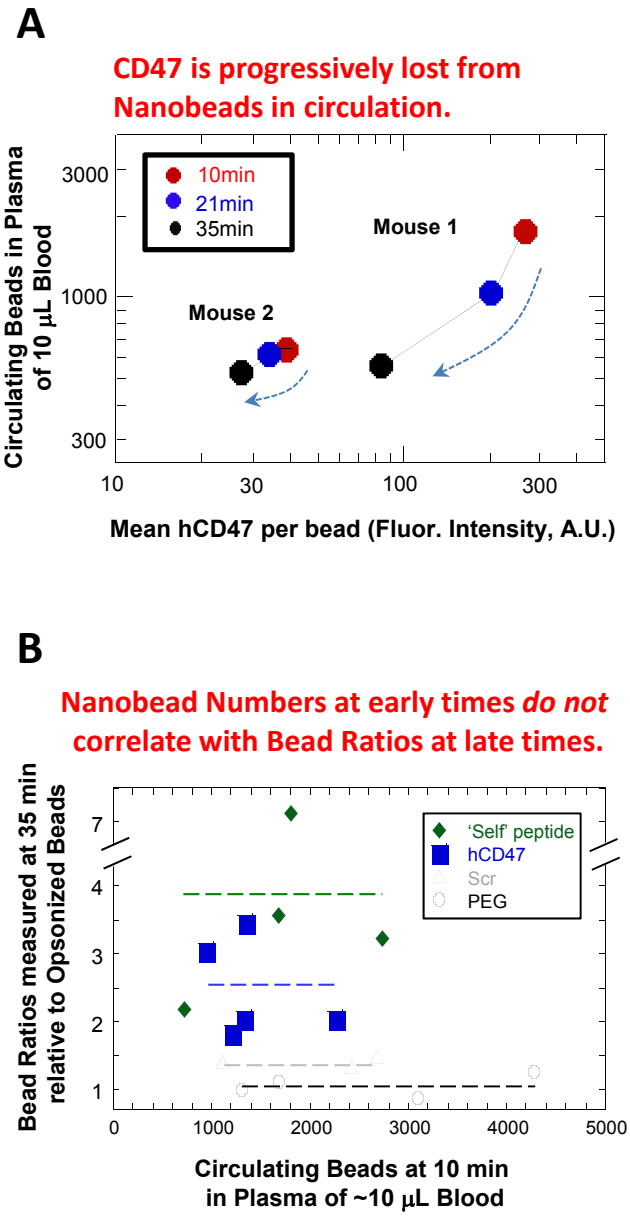
A
CD47 is progressively lost from Nanobeads in circulation.
10min
21min
35min
Mouse 1
Mouse 2
Circulating Beads in Plasma of 10 µL Blood
3000
1000
300
10
30
100
300
Mean hCD47 per bead (Fluor. Intensity, A.U.)
B
Nanobead Numbers at early times do not correlate with Bead Ratios at late times.
'Self' peptide
hCD47
Scr
PEG
Bead Ratios measured at 35 min relative to Opsonized Beads
7
4
3
2
1
0
1000
2000
3000
4000
5000
Circulating Beads at 10 min in Plasma of ~10 µL Blood

Figure S7

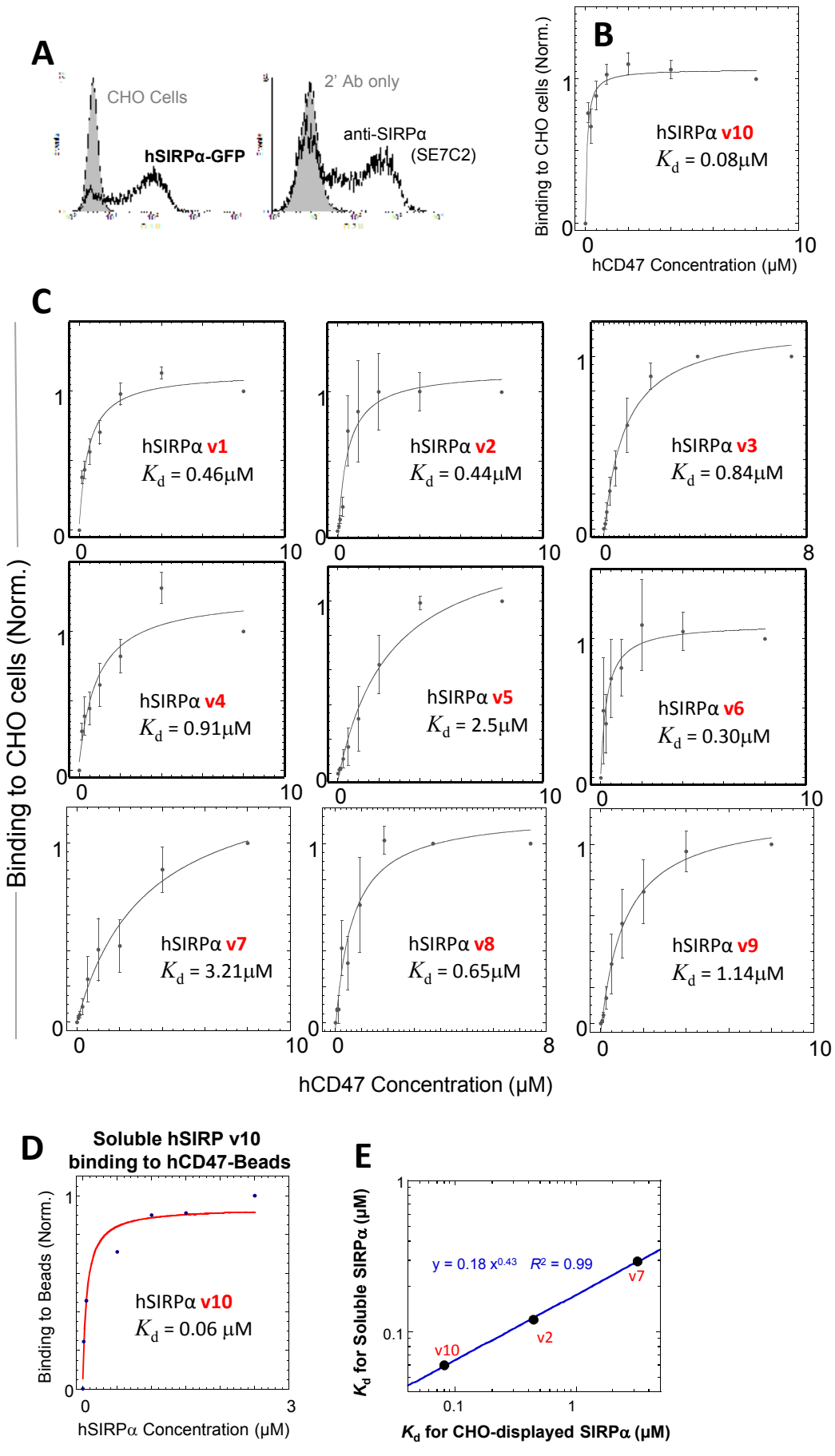
hSIRPα variants exhibit different affinities for hCD47
A
CHO Cells
hSIRPα-GFP
2' Ab only
anti-SIRPα
(SE7C2)
B
Binding to CHO cells (Norm.)
hSIRPα v10
K_d = 0.08μM
hCD47 Concentration (μM)
C
hSIRPα v1
K_d = 0.46μM
hSIRPα v2
K_d = 0.44μM
hSIRPα v3
K_d = 0.84μM
hSIRPα v4
K_d = 0.91μM
hSIRPα v5
K_d = 2.5μM
hSIRPα v6
K_d = 0.30μM
hSIRPα v7
K_d = 3.21μM
hSIRPα v8
K_d = 0.65μM
hSIRPα v9
K_d = 1.14μM
Binding to CHO cells (Norm.)
hCD47 Concentration (μM)
D
Soluble hSIRP v10
binding to hCD47-Beads
Binding to Beads (Norm.)
hSIRPα v10
K_d = 0.06 μM
hSIRPα Concentration (μM)
E
y = 0.18 x^0.43 R² = 0.99
v10
v2
v7
K_d for Soluble SIRPα (μM)
K_d for CHO-displayed SIRPα (μM)

Figure S8

Molecular Dynamics Simulations of Structures reveal Folding and Interactions

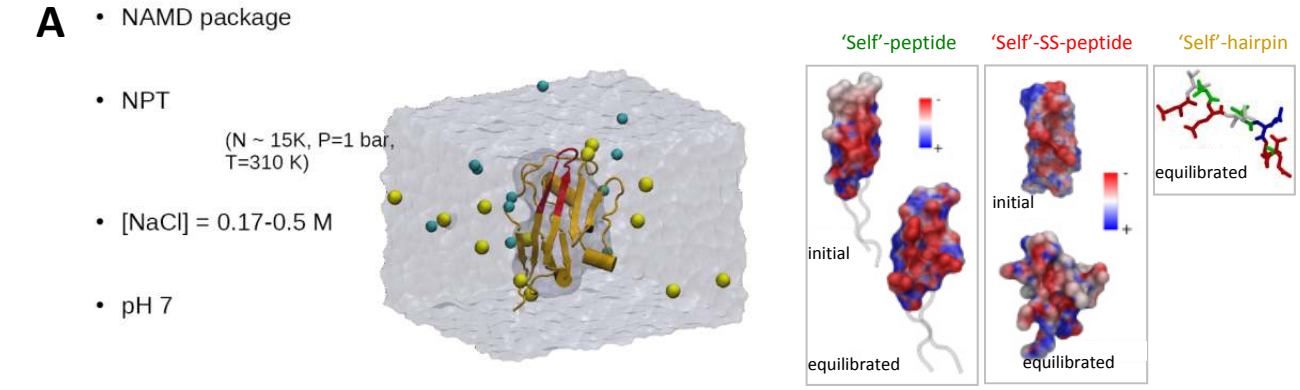

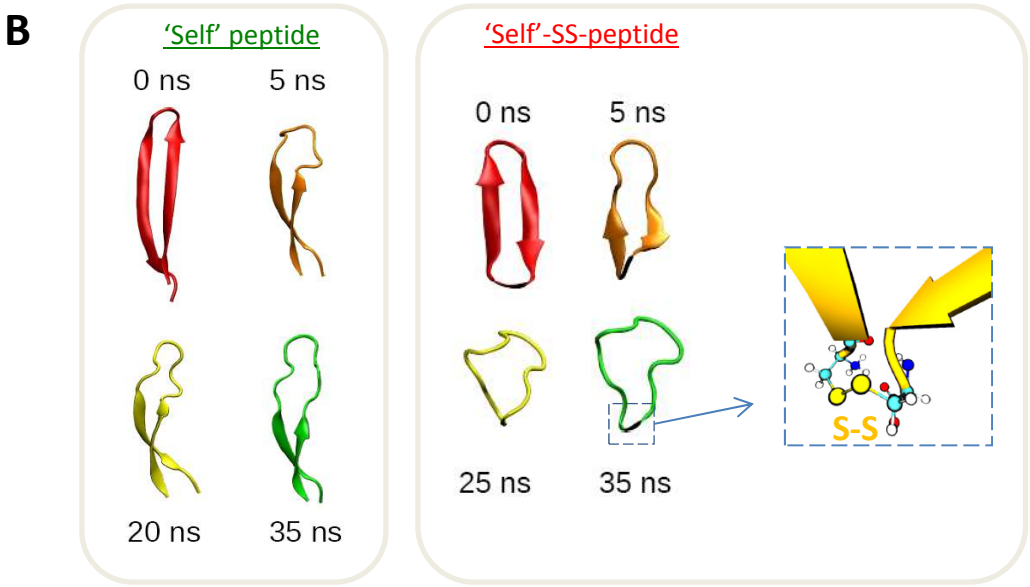

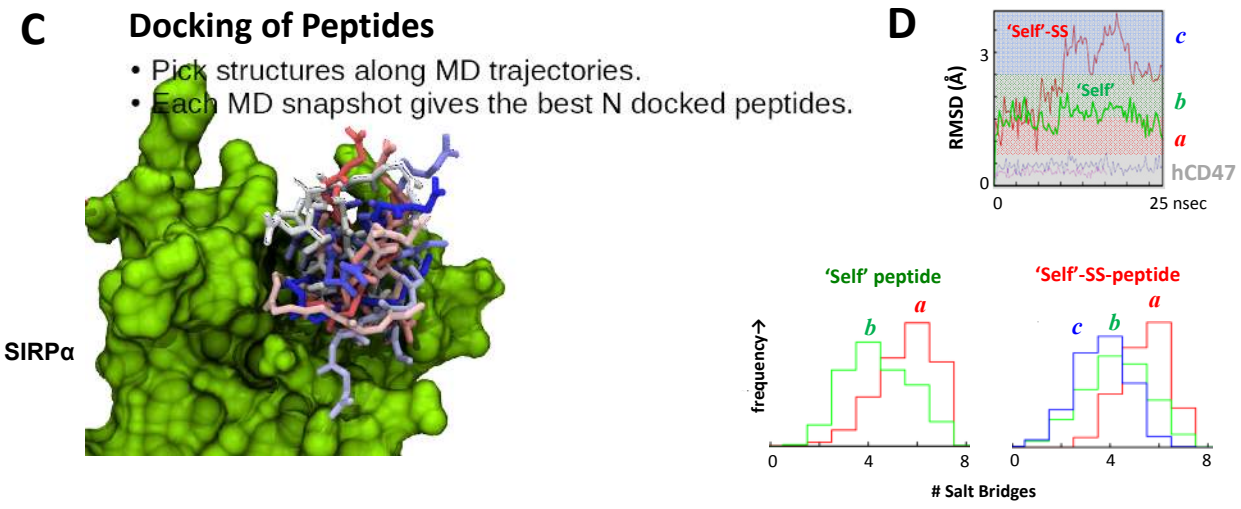

Figure S9

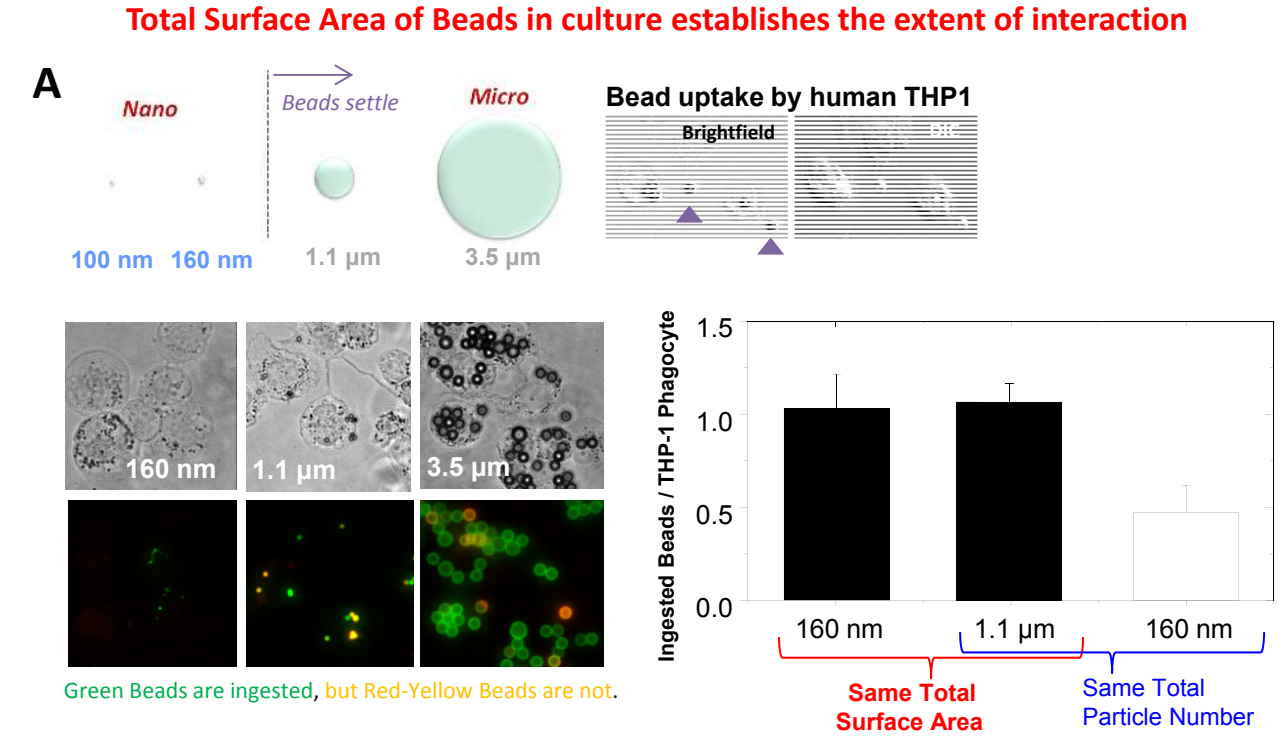
Total Surface Area of Beads in culture establishes the extent of interaction
A
Nano
Beads settle
Micro
100 nm
160 nm
1.1 µm
3.5 µm
Bead uptake by human THP1
Brightfield
160 nm
1.1 µm
3.5 µm
Green Beads are ingested, but Red-Yellow Beads are not.
Ingested Beads / THP-1 Phagocyte
1.5
1.0
0.5
0.0
160 nm
1.1 µm
160 nm
Same Total Surface Area
Same Total Particle Number

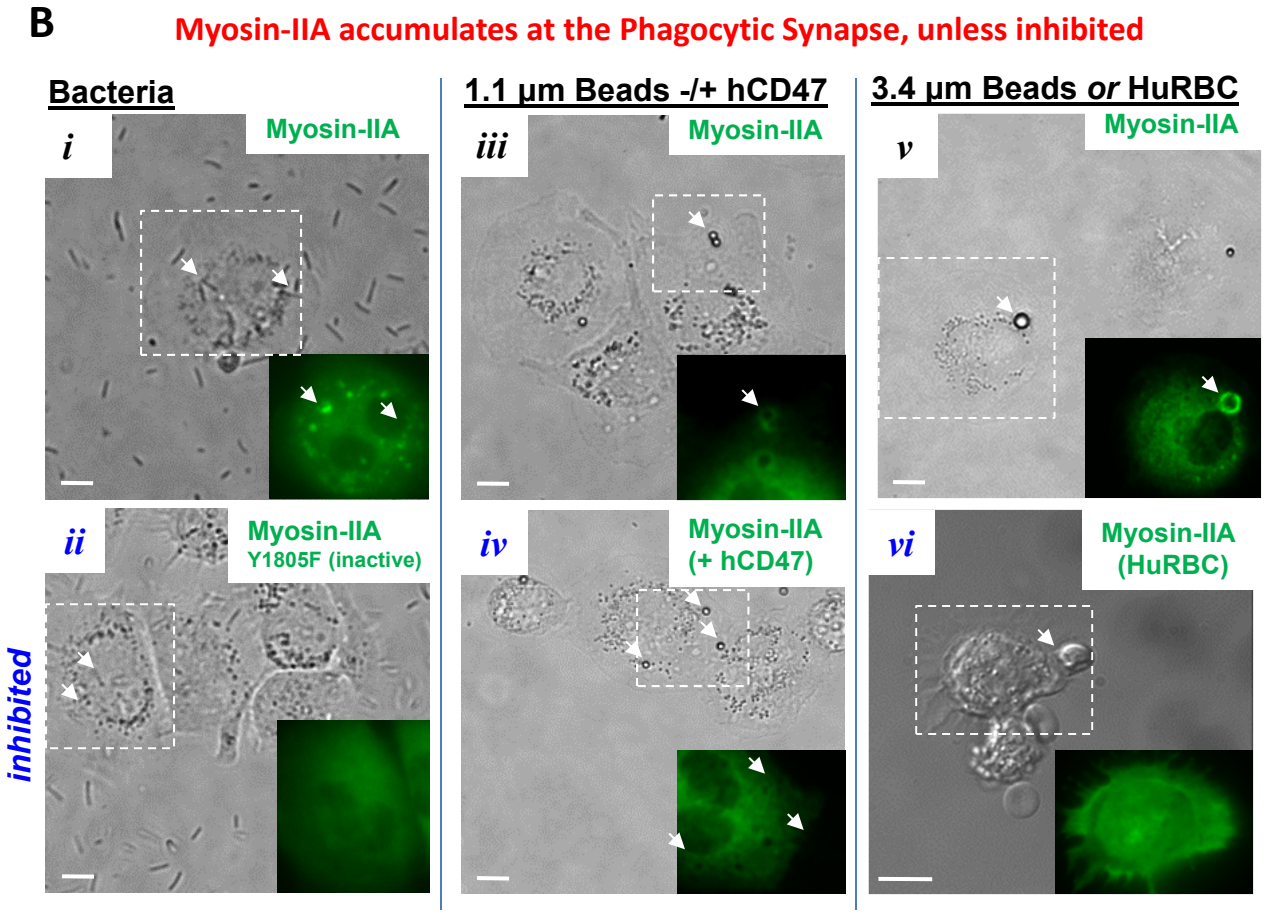
B
Myosin-IIA accumulates at the Phagocytic Synapse, unless inhibited
Bacteria
1.1 µm Beads -/+ hCD47
3.4 µm Beads or HuRBC
i
Myosin-IIA
iii
Myosin-IIA
v
Myosin-IIA
ii
Myosin-IIA
Y1805F (inactive)
iv
Myosin-IIA
(+ hCD47)
vi
Myosin-IIA
(HuRBC)
inhibited

Figure S9

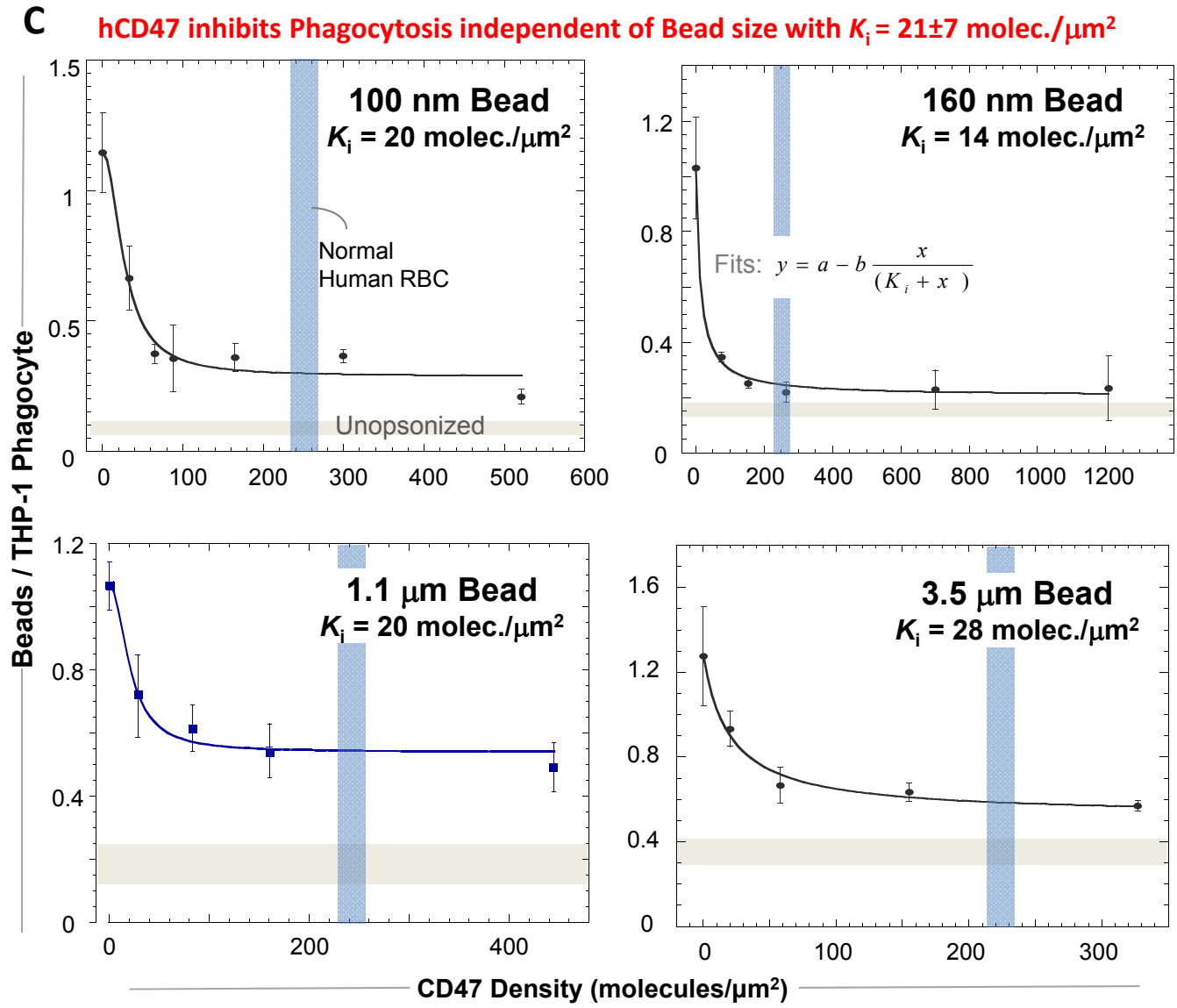
C
hCD47 inhibits Phagocytosis independent of Bead size with K_i = 21±7 molec./μm²
100 nm Bead
K_i = 20 molec./μm²
Normal
Human RBC
Unopsonized
160 nm Bead
K_i = 14 molec./μm²
Fits: $y = a - b\frac{x}{(K_i + x)}$
1.1 μm Bead
K_i = 20 molec./μm²
3.5 μm Bead
K_i = 28 molec./μm²
Beads / THP-1 Phagocyte
CD47 Density (molecules/μm²)

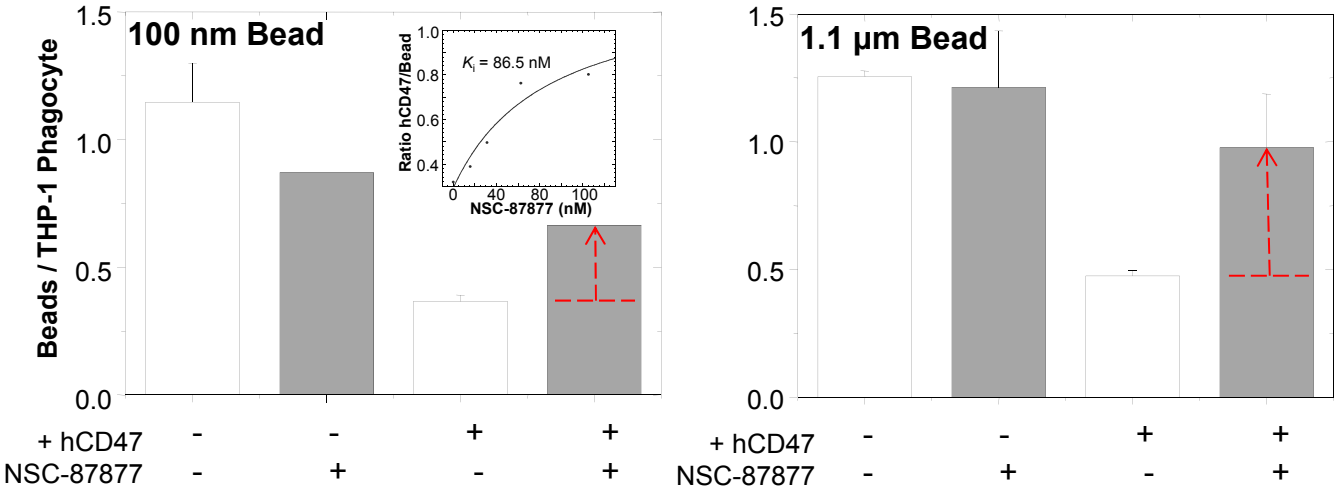
D
hCD47 signaling depends on SHP1 phosphatase
100 nm Bead
K_i = 86.5 nM
Ratio hCD47/Bead
NSC-87877 (nM)
1.1 μm Bead
Beads / THP-1 Phagocyte
+ hCD47
NSC-87877

Figure S10

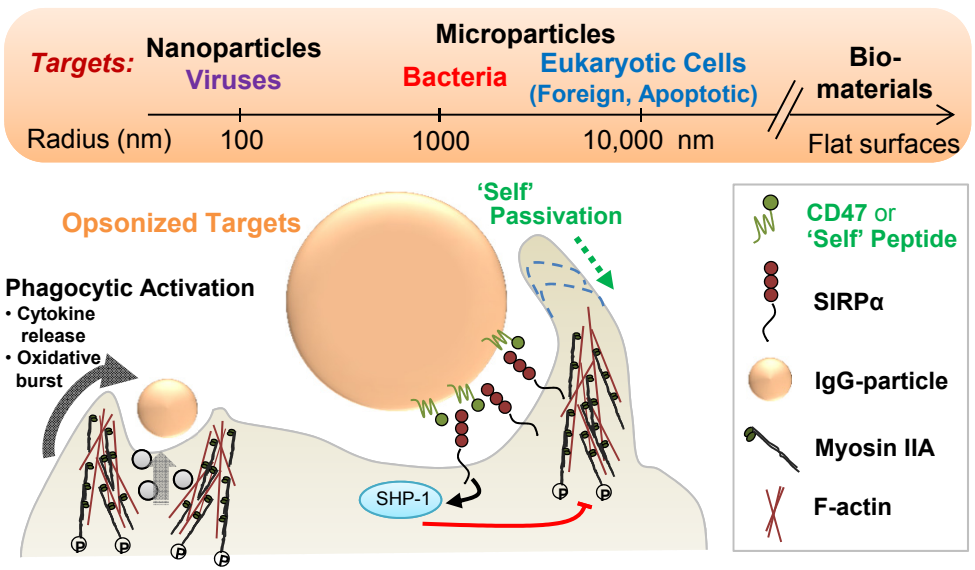
Targets:
Nanoparticles
Viruses
Microparticles
Bacteria
Eukaryotic Cells
(Foreign, Apoptotic)
Bio-
materials
Radius (nm)
100
1000
10,000 nm
Flat surfaces
Opsonized Targets
'Self'
Passivation
Phagocytic Activation
• Cytokine release
• Oxidative burst
SHP-1
CD47 or
'Self' Peptide
SIRPα
IgG-particle
Myosin IIA
F-actin

Table S1. Summary of a wide range of PEGylated particles that are opsonized. IgG is among the 3-4 most frequent opsonizing serum proteins (*32*), and complement is included because CD47 is also an effective inhibitor of complement mediated uptake [-(*8*) in text].

Table S1

PEGylated particles and Cells are invariably opsonized by serum proteins over time

PEG-Particle or RBC	IgG or complement* opsonized?	Reference (from most recent)
PEG-nevirapine	yes	R. Shegokar, ... R. H. Muller Nanomed. Nanotechnol., Biol. Med., 2011, 7, 333–340
Polymersomes, PEG-PBD	yes*	D.E. Discher … F. Ahmed Progress in Polymer Science, 2007, 32, 838-857
PEG-PCL	yes*	C. Lemarchand, ... P. Couvreur Biomaterials, 2006, 27, 108–118
Poloxamer-stabilized liposome	yes	T. M. Goppert and R. H. Muller. Int. J. Pharm., 2005, 302,172–186
	yes	S. Tamilvanan, ... S. Benita Eur. J. Pharm. Biopharm., 2005, 59, 1–7
PEG-PHDCA	yes	H. R. Kim, ... M. Taverna Electrophoresis, 2007, 28, 2252–2261
	yes	H. R. Kim, … P. Couvreur Biomacromolecules, 2007, 8, 793–799
	yes	M. T. Peracchia, ... P. Couvreur Biomaterials, 1999, 20, 1269–1275
PEG-PLA-PEG	yes*	M. Luck, ... T. Kissel J. Controlled Release, 1998, 55, 107–120
PEG-coated latex	yes*	M. Lu¨ck, ... R. H. Muller J. Biomed. Mater. Res., 1998, 39, 478–485
Poloxamer-coated polystyrene	yes	T. Blunk, ... R. H. Muller Electrophoresis, 1993, 14, 1382–1387
RBC	yes	Turrini, F. Mannu, P. Arese, J. Yuan, P. S. Low, 1993, Blood 81, 3146.

References

1. D. W. Bartlett, H. Su, I. J. Hildebrandt, W. A. Weber, M. E. Davis, Impact of tumor-specific targeting on the biodistribution and efficacy of siRNA nanoparticles measured by multimodality in vivo imaging. *Proc. Natl. Acad. Sci. U.S.A.* **104**, 15549 (2007). doi:10.1073/pnas.0707461104 Medline

2. A. L. Klibanov, K. Maruyama, A. M. Beckerleg, V. P. Torchilin, L. Huang, Activity of amphipathic poly(ethylene glycol) 5000 to prolong the circulation time of liposomes depends on the liposome size and is unfavorable for immunoliposome binding to target. *Biochim. Biophys. Acta* **1062**, 142 (1991). doi:10.1016/0005-2736(91)90385-L Medline

3. P. J. Photos, L. Bacakova, B. Discher, F. S. Bates, D. E. Discher, Polymer vesicles in vivo: Correlations with PEG molecular weight. *J. Control. Release* **90**, 323 (2003). doi:10.1016/S0168-3659(03)00201-3 Medline

4. R. L. Hong *et al*., Direct comparison of liposomal doxorubicin with or without polyethylene glycol coating in C-26 tumor-bearing mice: Is surface coating with polyethylene glycol beneficial? *Clin. Cancer Res.* **5**, 3645 (1999). Medline

5. R. Rossin, S. Muro, M. J. Welch, V. R. Muzykantov, D. P. Schuster, In vivo imaging of 64Cu-labeled polymer nanoparticles targeted to the lung endothelium. *J. Nucl. Med.* **49**, 103 (2008). doi:10.2967/jnumed.107.045302 Medline

6. J. K. Armstrong *et al*., Antibody against poly(ethylene glycol) adversely affects PEG-asparaginase therapy in acute lymphoblastic leukemia patients. *Cancer* **110**, 103 (2007). doi:10.1002/cncr.22739 Medline

7. M. J. Turk, D. J. Waters, P. S. Low, Folate-conjugated liposomes preferentially target macrophages associated with ovarian carcinoma. *Cancer Lett.* **213**, 165 (2004). doi:10.1016/j.canlet.2003.12.028 Medline

8. P. A. Oldenborg *et al*., Role of CD47 as a marker of self on red blood cells. *Science* **288**, 2051 (2000). doi:10.1126/science.288.5473.2051 Medline

9. A. A. Bentley, J. C. Adams, The evolution of thrombospondins and their ligand-binding activities. *Mol. Biol. Evol.* **27**, 2187 (2010). doi:10.1093/molbev/msq107 Medline

10. E. J. Brown, W. A. Frazier, Integrin-associated protein (CD47) and its ligands. *Trends Cell Biol.* **11**, 130 (2001). doi:10.1016/S0962-8924(00)01906-1 Medline

11. L. J. Bruce *et al*., A band 3-based macrocomplex of integral and peripheral proteins in the RBC membrane. *Blood* **101**, 4180 (2003). doi:10.1182/blood-2002-09-2824 Medline

12. I. Mouro-Chanteloup *et al*., Evidence that the red cell skeleton protein 4.2 interacts with the Rh membrane complex member CD47. *Blood* **101**, 338 (2003). doi:10.1182/blood-2002-04-1285 Medline

13. S. Subramanian, R. Parthasarathy, S. Sen, E. T. Boder, D. E. Discher, Species- and cell type-specific interactions between CD47 and human SIRPalpha. *Blood* **107**, 2548 (2006). doi:10.1182/blood-2005-04-1463 Medline

14. K. Takenaka *et al*., Polymorphism in *Sirpa* modulates engraftment of human hematopoietic stem cells. *Nat. Immunol.* **8**, 1313 (2007). doi:10.1038/ni1527 Medline

15. T. Strowig *et al*., Transgenic expression of human signal regulatory protein alpha in Rag2$^{-/-}$gamma(c)$^{-/-}$ mice improves engraftment of human hematopoietic cells in humanized mice. *Proc. Natl. Acad. Sci. U.S.A.* **108**, 13218 (2011). doi:10.1073/pnas.1109769108 Medline

16. R. K. Tsai, D. E. Discher, Inhibition of "self" engulfment through deactivation of myosin-II at the phagocytic synapse between human cells. *J. Cell Biol.* **180**, 989 (2008). doi:10.1083/jcb.200708043 Medline

17. F. Turrini, F. Mannu, P. Arese, J. Yuan, P. S. Low, Characterization of the autologous antibodies that opsonize erythrocytes with clustered integral membrane proteins. *Blood* **81**, 3146 (1993). Medline

18. D. Wilflingseder *et al*., IgG opsonization of HIV impedes provirus formation in and infection of dendritic cells and subsequent long-term transfer to T cells. *J. Immunol.* **178**, 7840 (2007). Medline

19. M. Lundqvist *et al*., Nanoparticle size and surface properties determine the protein corona with possible implications for biological impacts. *Proc. Natl. Acad. Sci. U.S.A.* **105**, 14265 (2008). doi:10.1073/pnas.0805135105 Medline

20. D. Cox, S. Greenberg, Phagocytic signaling strategies: Fc(gamma)receptor-mediated phagocytosis as a model system. *Semin. Immunol.* **13**, 339 (2001). doi:10.1006/smim.2001.0330 Medline

21. A. M. Glodek *et al*., Ligation of complement receptor 1 increases erythrocyte membrane deformability. *Blood* **116**, 6063 (2010). doi:10.1182/blood-2010-04-273904 Medline

22. D. Hatherley *et al*., Paired receptor specificity explained by structures of signal regulatory proteins alone and complexed with CD47. *Mol. Cell* **31**, 266 (2008). doi:10.1016/j.molcel.2008.05.026 Medline

23. S. Subramanian, E. T. Boder, D. E. Discher, Phylogenetic divergence of CD47 interactions with human signal regulatory protein alpha reveals locus of species specificity. Implications for the binding site. *J. Biol. Chem.* **282**, 1805 (2007). doi:10.1074/jbc.M603923200 Medline

24. I. C. MacDonald, E. E. Schmidt, A. C. Groom, The high splenic hematocrit: A rheological consequence of red cell flow through the reticular meshwork. *Microvasc. Res.* **42**, 60 (1991). doi:10.1016/0026-2862(91)90075-M Medline

25. Y. Matsumura, H. Maeda, A new concept for macromolecular therapeutics in cancer chemotherapy: Mechanism of tumoritropic accumulation of proteins and the antitumor agent smancs. *Cancer Res.* **46**, 6387 (1986). Medline

26. S. B. Willingham *et al*., The CD47-signal regulatory protein alpha (SIRPa) interaction is a therapeutic target for human solid tumors. *Proc. Natl. Acad. Sci. U.S.A.* **109**, 6662 (2012). doi:10.1073/pnas.1121623109 Medline

27. M. Seiffert *et al*., Human signal-regulatory protein is expressed on normal, but not on subsets of leukemic myeloid cells and mediates cellular adhesion involving its counterreceptor CD47. *Blood* **94**, 3633 (1999). Medline

28. J. A. Swanson, A. D. Hoppe, The coordination of signaling during Fc receptor-mediated phagocytosis. *J. Leukoc. Biol.* **76**, 1093 (2004). doi:10.1189/jlb.0804439 Medline

29. T. Matozaki, Y. Murata, H. Okazawa, H. Ohnishi, Functions and molecular mechanisms of the CD47-SIRPalpha signalling pathway. *Trends Cell Biol.* **19**, 72 (2009). doi:10.1016/j.tcb.2008.12.001 Medline

30. C. M. Cameron, J. W. Barrett, M. Mann, A. Lucas, G. McFadden, Myxoma virus M128L is expressed as a cell surface CD47-like virulence factor that contributes to the downregulation of macrophage activation in vivo. *Virology* **337**, 55 (2005). doi:10.1016/j.virol.2005.03.037 Medline

31. S. J. Stachelek *et al*., The effect of CD47 modified polymer surfaces on inflammatory cell attachment and activation. *Biomaterials* **32**, 4317 (2011). doi:10.1016/j.biomaterials.2011.02.053 Medline

32. C. D. Walkey, W. C. Chan, Understanding and controlling the interaction of nanomaterials with proteins in a physiological environment. *Chem. Soc. Rev.* **41**, 2780 (2012). doi:10.1039/c1cs15233e Medline

33. X. Zhang *et al*., Anti-tumor efficacy and biodistribution of intravenous polymeric micellar paclitaxel. *Anticancer Drugs* **8**, 696 (1997). doi:10.1097/00001813-199708000-00008 Medline

34. A. Ivetac, M. S. Sansom, Molecular dynamics simulations and membrane protein structure quality. *Eur. Biophys. J.* **37**, 403 (2008). doi:10.1007/s00249-007-0225-4 Medline

35. N. A. Baker, D. Sept, S. Joseph, M. J. Holst, J. A. McCammon, Electrostatics of nanosystems: Application to microtubules and the ribosome. *Proc. Natl. Acad. Sci. U.S.A.* **98**, 10037 (2001). doi:10.1073/pnas.181342398 Medline

36. W. Humphrey, A. Dalke, K. Schulten, VMD: Visual molecular dynamics. *J. Mol. Graph.* **14**, 33, 27 (1996). doi:10.1016/0263-7855(96)00018-5 Medline

37. C. Dominguez, R. Boelens, A. M. Bonvin, HADDOCK: A protein-protein docking approach based on biochemical or biophysical information. *J. Am. Chem. Soc.* **125**, 1731 (2003). doi:10.1021/ja026939x Medline

38. D. J. Barlow, J. M. Thornton, Ion-pairs in proteins. *J. Mol. Biol.* **168**, 867 (1983). doi:10.1016/S0022-2836(83)80079-5 Medline

39. G. Deplaine *et al*., The sensing of poorly deformable red blood cells by the human spleen can be mimicked in vitro. *Blood* **117**, e88 (2011). doi:10.1182/blood-2010-10-312801 Medline

40. M. Malmsten, K. Emoto, J. M. Van Alstine, Effect of chain density on inhibition of protein adsorption by poly(ethylene glycol) based coatings. *J. Colloid Interface Sci.* **202**, 507 (1998). doi:10.1006/jcis.1998.5513

41. D. A. Christian *et al*., Flexible filaments for in vivo imaging and delivery: Persistent circulation of filomicelles opens the dosage window for sustained tumor shrinkage. *Mol. Pharm.* **6**, 1343 (2009). doi:10.1021/mp900022m Medline

42. L. T. Baxter, H. Zhu, D. G. Mackensen, R. K. Jain, Physiologically based pharmacokinetic model for specific and nonspecific monoclonal antibodies and fragments in normal tissues and human tumor xenografts in nude mice. *Cancer Res.* **54**, 1517 (1994). Medline

43. R. K. Jain, Determinants of tumor blood flow: A review. *Cancer Res.* **48**, 2641 (1988). Medline

44. M. M. Tomayko, C. P. Reynolds, Determination of subcutaneous tumor size in athymic (nude) mice. *Cancer Chemother. Pharmacol.* **24**, 148 (1989). doi:10.1007/BF00300234 Medline